Available on the CERN CDS information server **CMS PAS SUS-16-033**

CMS Physics Analysis Summary

Contact: cms-pag-conveners-susy@cern.ch 2017/04/28

Search for supersymmetry in multijet events with missing transverse momentum in proton-proton collisions at 13 TeV

The CMS Collaboration

Abstract

A search for supersymmetry is presented based on multijet events with large missing transverse momentum produced in proton-proton collisions at center-of-mass energy $\sqrt{s} = 13$ TeV. The data, corresponding to an integrated luminosity of 35.9 fb^{-1}, were collected with the CMS detector at the CERN LHC in 2016. The analysis utilizes four-dimensional exclusive search regions defined in terms of the number of jets, the number of tagged bottom quark jets, the scalar sum of jet transverse momenta, and the magnitude of the vector sum of jet transverse momenta. No evidence for a significant excess of events is observed relative to the expectation from the standard model. Limits on the pair production of gluinos and squarks are derived in the context of simplified models. Assuming the lightest supersymmetric particle to be a weakly interacting neutralino, 95% confidence level lower limits on the gluino mass as large as 1800 to 1970 GeV are derived, and on the squark mass as large as 970 to 1450 GeV, depending on the production scenario.

This document has been revised with respect to the version dated March 24, 2017.

1 Introduction

The standard model (SM) of particle physics describes many aspects of weak, electromagnetic, and strong interactions. However, it requires unnatural fine tuning [1] to explain the observed value of the Higgs boson mass, and it does not offer an explanation for dark matter. Supersymmetry (SUSY) [2–9], a widely studied extension of the SM, potentially solves these problems through the introduction of a new particle, called a superpartner, for each SM particle, with a spin that differs from that of its SM counterpart by one half unit. The superpartners of quarks and gluons are squarks $\widetilde{\mathrm{q}}$ and gluinos $\widetilde{\mathrm{g}}$, respectively, while neutralinos $\widetilde{\chi}^0$ and charginos $\widetilde{\chi}^{\pm}$ are mixtures of the superpartners of Higgs and electroweak gauge bosons. Provided that the masses of gluinos, top squarks, and bottom squarks are no heavier than a few TeV, SUSY can resolve the fine-tuning problem [1, 10–12]. Furthermore, in R-parity [13] conserving SUSY models, the lightest SUSY particle (LSP) is stable and might interact only weakly, thus representing a dark matter candidate.

In this note, we present a search for squarks and gluinos produced in proton-proton (pp) collisions at $\sqrt{s} = 13\,\mathrm{TeV}$. The study is performed in the multijet final state, i.e., the visible elements consist solely of jets. Other $\sqrt{s} = 13\,\mathrm{TeV}$ inclusive multijet SUSY searches are presented in Refs. [14–19]. We assume the conservation of R-parity, meaning that the squarks and gluinos are produced in pairs. The events are thus characterized by the presence of jets and undetected, or "missing," transverse momentum, where the missing transverse momentum arises from the weakly interacting and unobserved LSPs. The data, corresponding to an integrated luminosity of $35.9\,\mathrm{fb}^{-1}$, were collected in 2016 with the CMS detector at the CERN LHC. The analysis is performed in four-dimensional exclusive intervals in the number of jets N_{jet}, the number of tagged bottom quark jets $N_{\text{b-jet}}$, the scalar sum H_{T} of the transverse momenta p_{T} of jets, and the magnitude $H_{\mathrm{T}}^{\mathrm{miss}}$ of the vector p_{T} sum of jets. The number of observed events in each interval is compared with the expected number of SM events to search for unexplained excesses in the data.

The study is an extension of that presented in Ref. [16], using improved analysis techniques and around 16 times more data. Relative to Ref. [16], the following principal modifications have been made. Firstly, the search intervals in N_{jet} and H_{T} are given by $N_{\mathrm{jet}} \geq 2$ and $H_{\mathrm{T}} > 300\,\mathrm{GeV}$, compared with $N_{\mathrm{jet}} \geq 4$ and $H_{\mathrm{T}} > 500\,\mathrm{GeV}$ in Ref. [16]. Inclusion of events with $N_{\mathrm{jet}} = 2$ and 3 increases the sensitivity to squark pair production. The lower threshold in H_{T} provides better sensitivity to scenarios with small mass differences between the LSP and the squark or gluino. Secondly, the rebalance-and-smear technique [20, 21] is introduced as a complementary means to evaluate the quantum chromodynamics (QCD) background, namely the background from SM events with multijet final states produced exclusively through the strong interaction. Thirdly, the search interval in $H_{\mathrm{T}}^{\mathrm{miss}}$ is given by $H_{\mathrm{T}}^{\mathrm{miss}} > 300\,\mathrm{GeV}$, rather than the previous $H_{\mathrm{T}}^{\mathrm{miss}} > 200\,\mathrm{GeV}$, in order to reserve the $250 < H_{\mathrm{T}}^{\mathrm{miss}} < 300\,\mathrm{GeV}$ region, not sensitive to signal event production, for a QCD data control sample. A final principal change is that finer segmentation is used to define exclusive intervals in H_{T} and $H_{\mathrm{T}}^{\mathrm{miss}}$ than in Ref. [16], to profit from the increased sensitivity afforded by the larger data sample.

Gluino and squark pair production are studied in the context of simplified models [22–25]. For gluino pair production, the T1tttt, T1bbbb, T1qqqq, T1tbtb, and T5qqqqVV [26] simplified models are considered, defined as follows. In the T1tttt scenario [Fig. 1 (upper left)], each gluino decays to a top quark-antiquark ($\mathrm{t\bar{t}}$) pair and the lightest neutralino $\widetilde{\chi}_1^0$, taken to be the weakly interacting LSP. The T1bbbb and T1qqqq scenarios are the same as the T1tttt scenario except with the $\mathrm{t\bar{t}}$ pairs replaced by bottom quark-antiquark ($\mathrm{b\bar{b}}$) or light-flavored (u, d, s, c) quark-antiquark ($\mathrm{q\bar{q}}$) pairs, respectively. In the T1tbtb scenario [Fig. 1 (upper right)], each

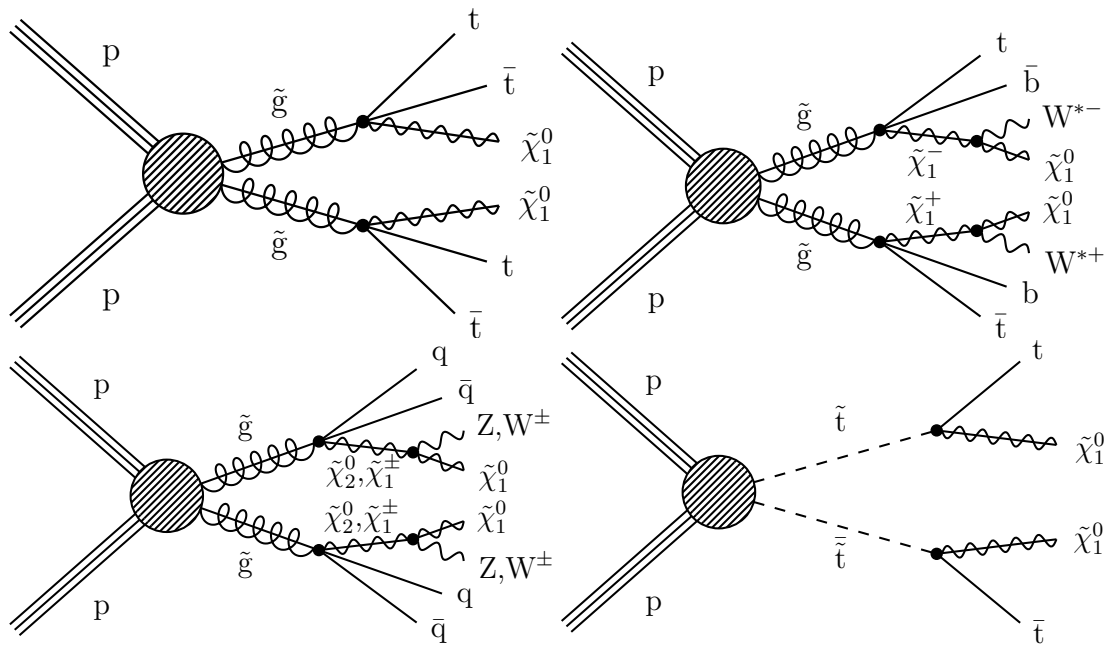

Figure 1: Example event diagrams for the simplified model signal scenarios considered in this study: the (upper left) T1tttt, (upper right) T1tbtb, (lower left) T5qqqqVV, and (lower right) T2tt scenarios. In the T5qqqqVV model, the flavor of the quark q and antiquark $\bar{q}$ differ from each other if the gluino $\tilde{g}$ decays as $\tilde{g} \to q\bar{q}\tilde{\chi}_1^{\pm}$, where $\tilde{\chi}_1^{\pm}$ is the lightest chargino.

gluino decays either as $\tilde{g} \to \bar{t}b\tilde{\chi}_1^+$ or as its charge conjugate, each with 50% probability, where $\tilde{\chi}_1^{\pm}$ denotes the lightest chargino. The $\tilde{\chi}_1^{\pm}$ is assumed to be nearly degenerate in mass with the $\tilde{\chi}_1^0$, representing the expected situation should the $\tilde{\chi}_1^{\pm}$ and $\tilde{\chi}_1^0$ appear within the same SU(2) multiplet [25]. The chargino subsequently decays to the $\tilde{\chi}_1^0$ LSP and to an off-shell W boson. In the T5qqqqVV scenario [Fig. 1 (lower left)], each gluino decays to a light-flavored $q\bar{q}$ pair and either to the next-to-lightest neutralino $\tilde{\chi}_2^0$ or to the $\tilde{\chi}_1^{\pm}$. The probability for the decay to proceed via the $\tilde{\chi}_2^0$, $\tilde{\chi}_1^+$, or $\tilde{\chi}_1^-$ is 1/3 for each possibility. The $\tilde{\chi}_2^0$ ($\tilde{\chi}_1^{\pm}$) subsequently decays to the $\tilde{\chi}_1^0$ LSP and to an on- or off-shell Z ($W^{\pm}$) boson.

We also consider models in which more than one of the decays $\tilde{g} \to t\bar{t}\tilde{\chi}_1^0$, $\tilde{g} \to b\bar{b}\tilde{\chi}_1^0$, and $\tilde{g} \to \bar{t}b\tilde{\chi}_1^+$ (or its charge conjugate) can occur [25]. Taken together, these scenarios reduce the model dependence of the assumptions for gluino decay to third-generation flavors. Specifically, we consider the following three mixed scenarios, with the respective branching fractions in parentheses:

- $\tilde{g} \to \bar{t}b\tilde{\chi}_1^+$ (25%), $\tilde{g} \to t\bar{b}\tilde{\chi}^-$ (25%), $\tilde{g} \to t\bar{t}\tilde{\chi}_1^0$ (50%);
- $\tilde{g} \to \bar{t}b\tilde{\chi}_1^+$ (25%), $\tilde{g} \to t\bar{b}\tilde{\chi}^-$ (25%), $\tilde{g} \to b\bar{b}\tilde{\chi}_1^0$ (50%);
- $\tilde{g} \to \bar{t}b\tilde{\chi}_1^+$ (25%), $\tilde{g} \to t\bar{b}\tilde{\chi}^-$ (25%), $\tilde{g} \to t\bar{t}\tilde{\chi}_1^0$ (25%), $\tilde{g} \to b\bar{b}\tilde{\chi}_1^0$ (25%).

The first scenario represents a mixture of the T1tbtb, T1tbtt, and T1tttt topologies; the second of the T1tbtb, T1tbbb, and T1bbbb topologies; and the third of the T1tbtb, T1tbbb, T1tbtt, T1bbtt, T1bbbb, and T1tttt topologies.

For squark-antisquark production, three simplified models are considered, denoted T2tt, T2bb, and T2qq. In the T2tt scenario [Fig. 1 (lower right)], top squark-antisquark production is followed by the decay of each squark to a top quark and the $\tilde{\chi}_1^0$ LSP. The T2bb and T2qq scenarios are the same as the T2tt scenario except with bottom squarks and quarks, or light-flavored squarks and quarks, respectively, in place of the top squarks and quarks.

All SUSY particles except those that participate in the respective reaction are assumed to have infinite mass, and the gluino is taken to decay promptly.

Background from SM processes arises from events with a top quark (either $\mathrm{t\bar{t}}$ events or events with a single top quark), events with jets and an on- or off-shell W or Z boson (W+jets and Z+jets events, respectively), and QCD events. Top quark and W+jets events can exhibit significant $H_{\mathrm{T}}^{\mathrm{miss}}$ and thus contribute to the background if a W boson decays to a neutrino and an undetected or out-of-acceptance charged lepton. Similarly, Z+jets events can exhibit significant $H_{\mathrm{T}}^{\mathrm{miss}}$ if the Z boson decays to two neutrinos. Significant $H_{\mathrm{T}}^{\mathrm{miss}}$ in QCD events is mostly the consequence of mismeasured jet p_{T}, but it can also arise if an event contains a charm or bottom quark that decays semileptonically.

2 Detector and trigger

A detailed description of the CMS detector, along with a definition of the coordinate system and pertinent kinematic variables, is given in Ref. [27]. Briefly, a cylindrical superconducting solenoid with an inner diameter of 6 m provides a 3.8 T axial magnetic field. Within the cylindrical volume are a silicon pixel and strip tracker, a lead tungstate crystal electromagnetic calorimeter (ECAL), and a brass and scintillator hadron calorimeter (HCAL). The tracking detectors cover the pseudorapidity range $|\eta| < 2.5$. The ECAL and HCAL, each composed of a barrel and two endcap sections, cover $|\eta| < 3.0$. Forward calorimeters extend the coverage to $3.0 < |\eta| < 5.0$. Muons are measured within $|\eta| < 2.4$ by gas-ionization detectors embedded in the steel flux-return yoke outside the solenoid. The detector is nearly hermetic, permitting accurate measurements of $H_{\mathrm{T}}^{\mathrm{miss}}$.

The CMS trigger is described in Ref. [28]. For this analysis, signal event candidates are recorded with triggers based on thresholds on missing transverse momentum. The efficiency of this trigger, which exceeds 98% following application of the event selection criteria described below, is measured in data and is taken into account in the analysis. Additional triggers, requiring the presence of charged leptons, photons, or minimum values of H_{T}, are used to select samples employed in the evaluation of backgrounds, as described below.

3 Event reconstruction

Individual particles are reconstructed with the CMS particle-flow (PF) algorithm [29, 30], which identifies them as photons, charged hadrons, neutral hadrons, electrons, or muons. To improve the quality of electron candidates [31], additional criteria are imposed on the ECAL shower shape and on the ratio of associated energies in the HCAL and ECAL. Analogously, for muon candidates [32], more stringent requirements are imposed on the matching between silicon-tracker and muon-detector track segments. Electron and muon candidates are restricted to $|\eta| < 2.5$ and <2.4, respectively.

The reconstructed vertex with the largest value of summed charged-track p_{T}^2 is taken to be the primary pp interaction vertex, and is required to lie within 24 cm of the center of the detector in the direction along the beam axis and 2 cm in the plane transverse to that axis. Charged tracks associated with vertices other than the primary vertex are removed.

To suppress jets erroneously identified as leptons and genuine leptons from hadron decays, electron and muon candidates are subjected to an isolation requirement. The isolation criterion is based on the variable I, which is the scalar p_{T} sum of PF charged hadrons, neutral hadrons, and photons within a cone of radius $\sqrt{(\Delta\phi)^2 + (\Delta\eta)^2}$ around the lepton direction, divided by

the lepton p_T, where ϕ is the azimuthal angle. The sum excludes the lepton candidate under consideration. The expected contributions of neutral particles from extraneous pp interactions (pileup) are subtracted [33]. The radius of the cone is 0.2 for lepton $p_T \leq 50\,\text{GeV}$, $10\,\text{GeV}/p_T$ for $50 \leq p_T \leq 200\,\text{GeV}$, and 0.05 for $p_T > 200\,\text{GeV}$. The decrease in cone size with increasing lepton p_T accounts for the increased collimation of the decay products from the lepton's parent particle as the Lorentz boost of the parent particle increases [34]. The isolation requirement is $I < 0.1$ for electrons and < 0.2 for muons.

Charged tracks not identified as an isolated electron or muon are also subjected to an isolation requirement. To be identified as an isolated charged track, the scalar p_T sum of charged tracks in a cone of radius 0.3 around the track direction, divided by the track p_T, must be less than 0.2 if the track is identified as a PF electron or muon and less than 0.1 otherwise. The sum excludes the track under consideration. Isolated charged tracks are required to satisfy $|\eta| < 2.4$.

Jets are defined by clustering PF candidates using the anti-k_T jet algorithm [35, 36] with a distance parameter of 0.4. Jet quality criteria [37] are imposed to eliminate jets from spurious sources such as electronics noise. The jet energies are corrected for the nonlinear response of the detector [38] and to account for the expected contributions of neutral particles from pileup [39]. Jets are required to have $p_T > 30\,\text{GeV}$.

The identification of bottom quark jets (b jets) is performed using the combined secondary vertex algorithm (CSVv2) at the medium working point [40]. The signal efficiency for b jets with $p_T \approx 30\,\text{GeV}$ is 55%. The corresponding misidentification probability for gluon and light-flavor-quark jets is 1.6% and for charm quark jets 12%.

4 Event selection and search intervals

Events considered as signal candidates are required to satisfy:

- $N_{\text{jet}} \geq 2$, where jets must appear within $|\eta| < 2.4$;
- $H_T > 300\,\text{GeV}$, with H_T the scalar p_T sum of jets with $|\eta| < 2.4$;
- $H_T^{\text{miss}} > 300\,\text{GeV}$, with H_T^{miss} the magnitude of $\vec{H}_T^{\text{miss}}$, the negative of the vector p_T sum of jets with $|\eta| < 5$; an extended η range is used to calculate H_T^{miss} so that it better represents the total missing transverse momentum in an event;
- no identified, isolated electron or muon candidate with $p_T > 10\,\text{GeV}$;
- no isolated charged-particle track with $m_T < 100\,\text{GeV}$ and $p_T > 10\,\text{GeV}$ ($p_T > 5\,\text{GeV}$ if the track is identified as a PF electron or muon), where m_T is the transverse mass [41] formed from the $\vec{p}_T^{\text{miss}}$ and isolated-track p_T vector, with $\vec{p}_T^{\text{miss}}$ the negative of the vector p_T sum of all PF objects;
- $\Delta\phi_{H_T^{\text{miss}},j_i} > 0.5$ for the two highest p_T jets j_1 and j_2, with $\Delta\phi_{H_T^{\text{miss}},j_i}$ the azimuthal angle between $\vec{H}_T^{\text{miss}}$ and the p_T vector of jet j_i; if $N_{\text{jet}} \geq 3$, then $\Delta\phi_{H_T^{\text{miss}},j_i} > 0.3$ for the third highest p_T jet j_3; if $N_{\text{jet}} \geq 4$, then $\Delta\phi_{H_T^{\text{miss}},j_i} > 0.3$ for the fourth highest p_T jet j_4; all considered jets must have $|\eta| < 2.4$.

In addition, anomalous events with reconstruction failures or that are triggered by noise or beam halo interactions are removed [42]. A breakdown of the efficiency at different stages of the selection process for representative signal models is given in Tables A.1 and A.2 of Appendix A.

The isolated-track veto requirement suppresses events with a hadronically decaying τ lepton or with an isolated electron or muon that is not identified; the m_T requirement restricts

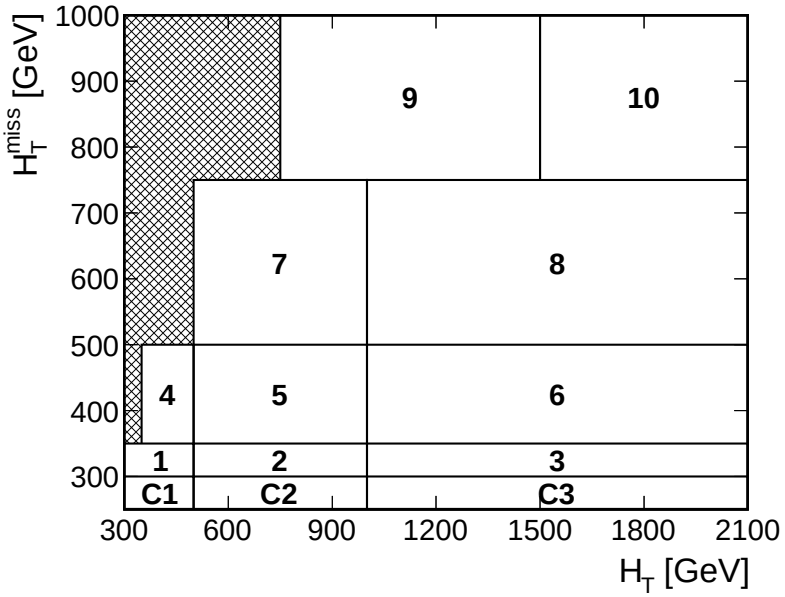

Figure 2: Schematic illustration of the 10 kinematic search intervals in the H_T^{miss} versus H_T plane. Intervals 1 and 4 are discarded for $N_{jet} \geq 7$. The intervals labeled C1, C2, and C3 are control regions used to evaluate the QCD background. The rightmost and topmost bins extend to $H_T = \infty$ and $H_T^{miss} = \infty$, respectively.

the isolated-track veto to situations consistent with W boson decay. The selection criteria on $\Delta\phi_{\vec{H}_T^{miss},j_i}$ suppress background from QCD events, for which $\vec{H}_T^{miss}$ is usually aligned along a jet direction.

The search is performed in four-dimensional exclusive intervals of N_{jet}, $N_{b\text{-}jet}$, H_T, and H_T^{miss}. The search intervals in N_{jet} and $N_{b\text{-}jet}$ are:

- N_{jet}: 2, 3–4, 5–6, 7–8, $\geq$9;
- $N_{b\text{-}jet}$: 0, 1, 2, $\geq$3.

Intervals with $N_{b\text{-}jet} \geq 3$ and $N_{jet} = 2$ are discarded since there are no entries. For H_T and H_T^{miss}, 10 kinematic intervals are defined, as specified in Table 1 and illustrated in Fig. 2. Events with both small H_T and large H_T^{miss} are not considered because such events are likely to arise from mismeasurement. For $N_{jet} \geq 7$, the kinematic intervals labeled 1 and 4 are discarded because of the small number of events. The total number of search intervals is 174.

The intervals labeled C1, C2, and C3 in Fig. 2 are control regions defined by $250 < H_T^{miss} < 300$ GeV, with the same boundaries in H_T as kinematic intervals 1, 2, and 3, respectively. These regions are used in the method to estimate the QCD background described in Section 7.3.2.

5 Simulated event samples

To evaluate the background, we mostly rely on data control regions, as discussed in Section 7. Samples of simulated SM events are used to validate the analysis procedures and for some secondary aspects of the background estimation. The SM production of $t\bar{t}$, W+jets, Z+jets, γ+jets, and QCD events is simulated using the MADGRAPH5_aMC@NLO 2.2.2 [43, 44] event generator at leading order (LO). The $t\bar{t}$ events are generated with up to three additional partons in the matrix element calculations, while up to four additional partons can be present for W+jets, Z+jets,

Table 1: Definition of the search intervals in the H_T^{miss} and H_T variables. Intervals 1 and 4 are discarded for $N_{jet} \geq 7$.

Interval	H_T^{miss} [GeV]	H_T [GeV]
1	300–350	300–500
2	300–350	500–1000
3	300–350	> 1000
4	350–500	350–500
5	350–500	500–1000
6	350–500	> 1000
7	500–750	500–1000
8	500–750	> 1000
9	> 750	750–1500
10	> 750	> 1500

and γ+jets events. Single top quark events in the s channel, diboson events such as WW, ZZ, and ZH production, with H a Higgs boson, and rare events such as $t\bar{t}W$, $t\bar{t}Z$, and WWZ production, are generated with this same program [43, 45] at next-to-leading (NLO) order, except that WW events in which both W bosons decay leptonically are generated using the POWHEG v2.0 [46–50] program at NLO. The POWHEG generator at NLO is also used to describe single top events in the t and tW channels. The detector response is modeled with the GEANT4 [51] suite of programs. Normalization of the simulated background samples is performed using the most accurate cross section calculations available [43, 49, 50, 52–60], which generally correspond to NLO or next-to-NLO precision.

Samples of simulated signal events are generated at LO using the MADGRAPH5_aMC@NLO program. Up to two additional partons are included in the matrix element calculation. The production cross sections are determined with NLO plus next-to-leading-logarithm (NLL) accuracy [61–65]. Events with gluino (squark) pair production are generated for a range of gluino $m_{\tilde{g}}$ (squark $m_{\tilde{q}}$) and LSP $m_{\tilde{\chi}_1^0}$ mass values, with $m_{\tilde{\chi}_1^0} < m_{\tilde{g}}$ ($m_{\tilde{\chi}_1^0} < m_{\tilde{q}}$). For the T1tbtb model, the mass of the intermediate $\tilde{\chi}_1^{\pm}$ state is taken to be $m_{\tilde{\chi}_1^0} + 5\,\text{GeV}$, while for the T5qqqqVV model, the masses of the intermediate $\tilde{\chi}_2^0$ and $\tilde{\chi}_1^{\pm}$ are given by the mean of $m_{\tilde{\chi}_1^0}$ and $m_{\tilde{g}}$. The gluinos and squarks decay according to phase space [66]. To render the computational requirements manageable, the detector response is described using the CMS fast simulation [67, 68], which yields consistent results with the GEANT4-based simulation, except that we apply a correction of 1% to account for differences in the efficiency of the jet quality requirements [37], corrections of 5–12% to account for differences in the b jet tagging efficiency, and corrections of 0–14% to account for differences in the modeling of H_T^{miss}.

For simulated samples generated at LO (NLO), the NNPDF3.0LO [69] (NNPDF3.0NLO [69]) parton distribution functions (PDFs) are used. Parton showering and hadronization are described by the PYTHIA 8.2 [66] program for all samples.

To improve the description of initial-state radiation (ISR), we compare the MADGRAPH prediction to data in a control region enriched in $t\bar{t}$ events: two leptons (ee, $\mu\mu$, or eμ) and two tagged b jets are required, implying that all other jets in the event arise from ISR. The correction factor is derived as a function of the number N_{jet}^{ISR} of ISR jets per event, with a central value ranging from 0.92 for $N_{jet}^{ISR} = 1$ to 0.51 for $N_{jet}^{ISR} \geq 6$. These corrections are applied to simulated $t\bar{t}$ and signal events. The associated systematic uncertainty is defined to be half the deviation from one of the correction.

Table 2: Systematic uncertainties in the selection efficiency of signal events, averaged over all search regions. The variations correspond to different signal models and choices for the SUSY particle masses. Results reported as 0.0 correspond to values less than 0.05%. "Mixed T1" refers to the mixed models of gluino decays to heavy squarks described in the introduction.

Item	Relative uncertainty (%)
Trigger efficiency	$0.2-2.8$
Jet quality requirements	1.0
Initial-state radiation	$0.0-14$
Renormalization and factorization scales	$0.0-6.2$
Jet energy scale	$0.0-7.7$
Jet energy resolution	$0.0-4.2$
MC statistical uncertainty	$1.5-30$
$H_{\mathrm{T}}^{\mathrm{miss}}$ modeling	$0.0-13$
Pileup	$0.2-5.5$
Isolated lepton & isolated track vetoes (T1tttt, T1tbtb, mixed T1, T5qqqqVV, and T2tt models)	2.0
Total	$3.9-34$

6 Signal systematic uncertainties

Systematic uncertainties in the signal event selection efficiency are listed in Table 2. To evaluate the uncertainty associated with the renormalization and factorization scales, each scale is varied independently by a factor of 2.0 and 0.5 [70, 71]. The uncertainties associated with the renormalization and factorization scales, and with ISR, integrated over all search regions, typically lie below 0.1% but can be as large as the maximum values noted in Table 2 for $\Delta m \approx 0$, where Δm is the difference between the gluino or squark mass and the sum of the masses of the particles into which it decays. For example, for the T1tttt model, Δm is given by $\Delta m = m_{\tilde{\mathrm{g}}} - (m_{\tilde{\chi}_1^0} + 2m_{\mathrm{top}})$, with m_{top} the top quark mass. The uncertainties associated with the jet energy scale and jet energy resolution are evaluated as a function of jet p_{T} and η. An uncertainty in the selection efficiency associated with pileup is evaluated based on the observed distribution of the number N_{vtx} of reconstructed vertices, and on the selection efficiency and its uncertainty determined from simulation as a function of N_{vtx}. The isolated lepton and isolated track vetoes have a minimal impact on the T1bbbb, T1qqqq, T2bb, and T2qq models because events in these models rarely contain an isolated lepton. Thus, the associated uncertainty is negligible ($\lesssim 0.1\%$).

Systematic uncertainties in the signal predictions associated with the b jet tagging and misidentification efficiencies are also evaluated. These uncertainties do not affect the selection efficiency but can potentially alter the shape of signal distributions. The systematic uncertainties associated with the trigger, renormalization and factorization scales, ISR, jet energy scale, jet energy resolution, statistical precision in the event samples, and $H_{\mathrm{T}}^{\mathrm{miss}}$ modeling can also affect the shapes of the signal distributions. We account for these potential changes in shape, i.e., migration of events between search regions, in the limit-setting procedure described in Section 8.

The systematic uncertainty in the determination of the integrated luminosity is 2.6% [72].

7 Background evaluation

The evaluation of background is primarily based on data control regions (CRs). Signal events, if present, could populate the CRs, an effect known as signal contamination. The impact of

signal contamination is evaluated as described in Section 8. Signal contamination is negligible for all CRs except those used to evaluate the top quark and W+jets background (Section 7.1). It is nonnegligible only for the models that can produce a non-isolated track or lepton, viz., the T1tttt, T1tbtb, T5qqqqVV, and T2tt models, and the mixed models of gluino decays to heavy squarks described in the introduction.

7.1 Background from top quark and W+jets events

The background from the SM production of $\mathrm{t\bar{t}}$, single top quark, and W+jets events originates from W bosons that decay leptonically to yield a neutrino and a charged lepton. If the charged lepton is an electron or muon, including those from τ lepton decay, it is called a "lost" lepton. A lost lepton arises if an electron or muon lies outside the analysis acceptance, is not reconstructed, or is not isolated, and thus is not vetoed by the requirements of Section 4. The other possibility is that the charged lepton is a hadronically decaying τ lepton, denoted "τ_{h}."

7.1.1 Lost-lepton background

The procedure used to evaluate the lost-lepton background is described in Ref. [16] (see also Refs. [20, 21, 73]). Briefly, single-lepton CRs are selected using the standard trigger and selection criteria, except with the electron and muon vetoes inverted and the isolated-track veto not applied. Exactly one isolated electron or muon must be present. In addition, the transverse mass m_{T} formed from the $\vec{p}_{\mathrm{T}}^{\,\mathrm{miss}}$ and lepton-p_{T} vector is required to satisfy $m_{\mathrm{T}} < 100\,\mathrm{GeV}$: this requirement is effective at identifying SM events while reducing signal contamination. The T1tttt (T1tbtb, T5qqqqVV, T2tt) signal contamination in the resulting CRs is generally negligible, viz., $\lesssim 0.1\%$, but it can be as large as 30–50% (25–60%, 2–15%, 5–50%) for large values of N_{jet}, $N_{\mathrm{b\text{-}jet}}$, H_{T}, and/or $H_{\mathrm{T}}^{\mathrm{miss}}$, depending on $m_{\tilde{\mathrm{g}}}$ or $m_{\tilde{\mathrm{q}}}$ and $m_{\tilde{\chi}_1^0}$. Generally similar results to the T1tbtb model are obtained for the mixed models of gluino decay to heavy squarks.

Each CR event is entered into one of the 174 search regions with a weight that represents the probability for a lost-lepton event to appear with the corresponding values of H_{T}, $H_{\mathrm{T}}^{\mathrm{miss}}$, N_{jet}, and $N_{\mathrm{b\text{-}jet}}$. The weights are determined from the $\mathrm{t\bar{t}}$, W+jets, single top quark, and rare process simulations through evaluation of the efficiency of the lepton acceptance, lepton reconstruction, lepton isolation, isolated-track, and m_{T} requirements. Corrections are applied to account for the purity of the CR, the contributions of dilepton events to the signal regions and CR, and efficiency differences with respect to data. More details are provided in Ref. [16]. The efficiencies are determined as a function of H_{T}, $H_{\mathrm{T}}^{\mathrm{miss}}$, N_{jet}, $N_{\mathrm{b\text{-}jet}}$, lepton p_{T} and η, and other kinematic variables. Improvements relative to Ref. [16] are that we now use $N_{\mathrm{b\text{-}jet}}$ and lepton η to help characterize the efficiencies, and the efficiency of the isolated-track veto is now determined separately for lost-lepton events that fail the acceptance, reconstruction, or isolation requirements, whereas previously only a single overall isolated-track veto efficiency was evaluated (as a function of search region) when constructing the weights.

The weighted distributions of the search variables, summed over the events in the CRs, define the lost-lepton background prediction. The procedure is performed separately for the single-electron and single-muon CRs, both of which are used to predict the total lost-lepton background, i.e., the background due both to lost electrons and to lost muons. The two independent predictions yield consistent results and are averaged to obtain the final lost-lepton background estimate. The method is checked with a closure test, namely by determining the ability of the method, applied to simulated event samples, to predict correctly the true number of background events. The results of this test are shown in the upper plot of Fig. 3.

The dominant uncertainty in the lost-lepton background prediction is statistical, due to the

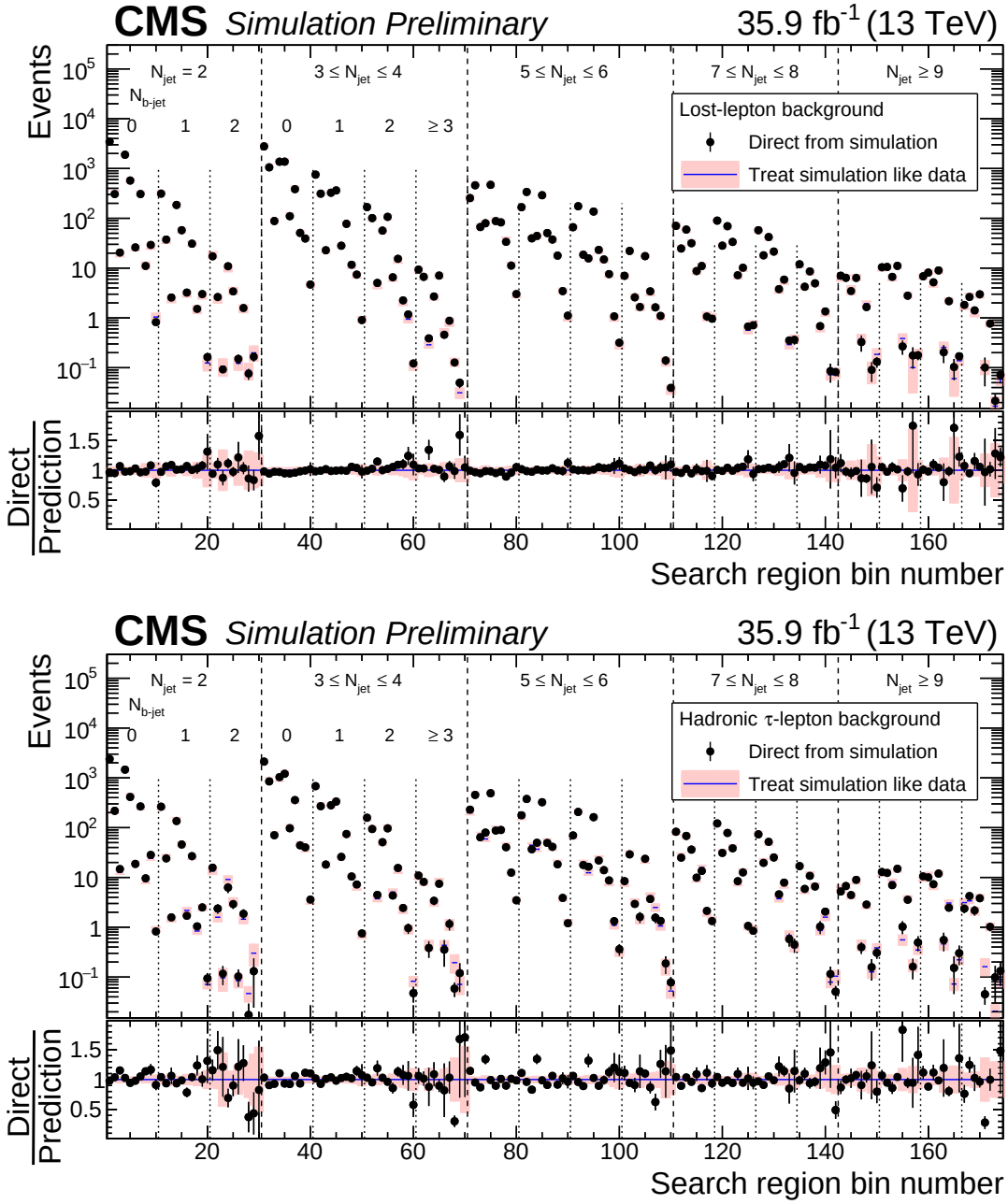

Figure 3: (Upper plot) The lost-lepton background in the 174 search regions of the analysis as determined directly from $t\bar{t}$, single top quark, W+jets, diboson, and rare-event simulation (points, with statistical uncertainties) and as predicted by applying the lost-lepton background determination procedure to simulated electron and muon control samples (histograms, with statistical uncertainties). The lower panel shows the ratio between the two sets of results. (Lower plot) The corresponding simulated results for the background from hadronically decaying τ leptons. For both plots, the 10 results (8 results for $N_{\text{jet}} \geq 7$) within each region delineated by vertical dashed lines correspond sequentially to the 10 (8) kinematic intervals of H_{T} and $H_{\text{T}}^{\text{miss}}$ indicated in Table 1 and Fig. 2.

limited number of CR events. As a systematic uncertainty, we take the larger of the observed nonclosure and the statistical uncertainty in the nonclosure, for each search region, where "nonclosure" refers to the difference between the solid points and histogram in Fig. 3 (upper plot). Additional systematic uncertainties are evaluated as described in Ref. [16] and account for potential differences between the data and simulation for the lepton acceptance, lepton reconstruction efficiency, lepton isolation efficiency, isolated track efficiency, m_{T} selection efficiency, dilepton contributions, and purity of the CRs.

7.1.2 Hadronically decaying τ lepton background

To evaluate the top quark and W+jets background due to τ_{h} events, a CR event sample is selected using a trigger that requires either at least one muon candidate with $p_{\mathrm{T}} > 24\,\mathrm{GeV}$, or at least one muon candidate with $p_{\mathrm{T}} > 15\,\mathrm{GeV}$ in conjunction with $H_{\mathrm{T}} > 500\,\mathrm{GeV}$. The reason a special trigger is used, and not the standard one, is that the τ_{h} background determination method requires there not be a selection requirement on missing transverse momentum (see below). The selected events are required to contain exactly one identified muon with $|\eta| < 2.1$. The p_{T} of the muon candidate must exceed 20 GeV, or 25 GeV if $H_{\mathrm{T}} < 500\,\mathrm{GeV}$. The fraction of T1tttt (T1tbtb, T5qqqqVV, T2tt) events in the CR due to signal contamination is generally $\lesssim 0.1\%$, but can be as large as 5–22% (1–20%, 1–15%, 1–40%) for large values of N_{jet}, $N_{\text{b-jet}}$, H_{T}, and/or $H_{\mathrm{T}}^{\text{miss}}$, depending on $m_{\tilde{\mathrm{g}}}$ or $m_{\tilde{\mathrm{q}}}$ and $m_{\tilde{\chi}_1^0}$, with similar results to the T1tbtb model for the mixed models of gluino decay to heavy squarks.

The τ_{h} background is determined using the method described in Ref. [16] (see also Refs. [20, 21, 73]). It makes use of the similarity between μ+jets and τ_{h}+jets events aside from the detector response to the μ or τ_{h}. In each CR event, the muon p_{T} is smeared through random sampling of τ_{h} response functions derived from simulation of single $\mathrm{W} \to \tau_{\mathrm{h}}\nu_\tau$ decay events (this differs from Ref. [16], in which $\mathrm{W} \to \tau_{\mathrm{h}}\nu_\tau$ decays in simulated $\mathrm{t\bar{t}}$ and W+jets events were used to derive the response functions). The response functions express the expected visible-p_{T} distribution of a τ_{h} candidate as a function of the true τ-lepton p_{T}, taken to be the measured muon p_{T} in the CR event. Following the smearing, the values of H_{T}, $H_{\mathrm{T}}^{\text{miss}}$, N_{jet}, and $N_{\text{b-jet}}$ are calculated for the CR event, and the selection criteria of Section 4 are applied. Note that CR events with relatively low values of $H_{\mathrm{T}}^{\text{miss}}$ can be promoted, after smearing, to have $H_{\mathrm{T}}^{\text{miss}}$ values above the nominal threshold, and thus appear in the τ_{h} background prediction. It is for this reason that the CR is selected using a trigger without a requirement on missing missing transverse momentum: to avoid possible $H_{\mathrm{T}}^{\text{miss}}$ bias. The misidentification probability for a τ_{h} jet to be erroneously identified as a b jet is taken into account. Corrections are applied to account for the trigger efficiency, the acceptance and efficiency of the μ selection, and the ratio of branching fractions $\mathcal{B}(\mathrm{W} \to \tau_{\mathrm{h}}\nu)/\mathcal{B}(\mathrm{W} \to \mu\nu) = 0.65$ [74]. The resulting event yield provides the τ_{h} background estimate. The method is validated with a closure test, whose results are shown in the lower plot of Fig. 3.

Systematic uncertainties are assigned based on the level of nonclosure, as described for the lost-lepton background. In addition, systematic uncertainties are evaluated for the muon reconstruction, isolation, and acceptance efficiencies, for the response functions, and for the misidentification rate of τ_{h} jets as b jets. The dominant source of uncertainty, as for the lost-lepton background, is from the limited statistical precision of the CR sample.

7.2 Background from $\mathrm{Z} \to \nu\bar{\nu}$ events

The evaluation of background from SM Z+jets events with $\mathrm{Z} \to \nu\bar{\nu}$ is based on CR samples of γ+jets events, and of Z+jets events with $\mathrm{Z} \to \ell^+\ell^-$ (ℓ = e, μ). The photon in the γ+jets

events and the $\ell^+\ell^-$ pair in the $Z \to \ell^+\ell^-$ events are removed from the event in order to emulate missing transverse momentum. The γ+jets and $Z \to \ell^+\ell^-$ events are then subjected to the same selection criteria as in the standard analysis, with corrections applied to account for differences in acceptance with respect to the $Z(\to \nu\overline{\nu})$+jets process. The use of γ+jets events exploits the similarity between Z boson and direct photon production in pp collisions, where "direct" refers to a photon produced through the Compton scattering ($qg \to q\gamma$) or annihilation ($q\overline{q} \to g\gamma$) process.

The method is an extension of that described in Ref. [16]. Briefly, the relatively copious γ+jets events are used to evaluate the background in the 46 search regions with $N_{\text{b-jet}} = 0$. We do not use γ+jets events for the $N_{\text{b-jet}} > 0$ search regions because of current limitations in event generators for the theoretical modeling of γ+jets versus Z+jets production with bottom quarks. The less abundant $Z \to \ell^+\ell^-$ events are used to validate and calibrate the $N_{\text{b-jet}} = 0$ results, as described below, and to extrapolate to the $N_{\text{b-jet}} > 0$ search regions. For this extrapolation, the $Z \to \ell^+\ell^-$ data are integrated over H_{T} and $H_{\text{T}}^{\text{miss}}$ because of the limited number of events.

The $Z \to \ell^+\ell^-$ CR sample is selected using a combination of triggers that requires either i) at least one isolated electron or muon with $p_{\text{T}} > 15\,\text{GeV}$, and either $H_{\text{T}} > 350\,\text{GeV}$ or $H_{\text{T}} > 400\,\text{GeV}$ depending on the LHC running conditions, ii) at least one electron with either $p_{\text{T}} > 105$ or $115\,\text{GeV}$ depending on the running conditions, iii) at least one muon with $p_{\text{T}} > 50\,\text{GeV}$, or iv) at least one isolated electron (muon) with $p_{\text{T}} > 27$ (24) GeV. The events are required to contain exactly one e^+e^- or one $\mu^+\mu^-$ pair with an invariant mass within 15 GeV of the nominal Z boson mass, with the constituents of the pair identified using the same criteria for isolated electrons and muons as in the standard analysis. The p_{T} of the lepton pair must exceed 200 GeV. So that the $Z \to \ell^+\ell^-$ and γ+jets CRs are independent, a veto is applied to events containing an identified photon.

The γ+jets CR sample is selected with a trigger that requires a photon candidate with $p_{\text{T}} > 175\,\text{GeV}$. The events are subsequently required to contain exactly one well-identified isolated photon with $p_{\text{T}} > 200\,\text{GeV}$. About 85% of the events in the resulting sample are estimated to contain a direct photon, while the remaining events either contain a fragmentation photon, i.e., emitted as ISR or during the hadronization process, or a non-prompt photon, i.e., from unstable hadron decay. A fit to the photon isolation variable is performed as a function of $H_{\text{T}}^{\text{miss}}$ to determine the photon purity β_γ, defined as the fraction of events in the γ+jets CR with a direct or fragmentation photon (these two types of photons are experimentally indistinguishable and together are referred to as "prompt").

The estimated number $N^{\text{pred}}_{Z\to\nu\overline{\nu}}$ of $Z(\to \nu\overline{\nu})$+jets background events contributing to each $N_{\text{b-jet}} = 0$ search region is given by:

$$N^{\text{pred}}_{Z\to\nu\overline{\nu}}\Big|_{N_{\text{b-jet}}=0} = \rho\mathcal{R}^{\text{sim}}_{Z\to\nu\overline{\nu}/\gamma}\mathcal{F}_{\text{dir}}\beta_\gamma N^{\text{obs}}_\gamma \,/\, \mathcal{C}^{\gamma}_{\text{data/sim}}, \tag{1}$$

where N^{obs}_γ is the number of events in the corresponding N_{jet}, H_{T}, and $H_{\text{T}}^{\text{miss}}$ bin of the γ+jets CR, β_γ is the fraction that are prompt, $\mathcal{F}_{\text{dir}}$ is the fraction of prompt photons that are also direct (evaluated from simulation), and $\mathcal{R}^{\text{sim}}_{Z\to\nu\overline{\nu}/\gamma}$ is the ratio from simulation of the number of $Z(\to \nu\overline{\nu})$+jets events to the number of direct-photon γ+jets events, with the direct photon term obtained from an LO MADGRAPH5_aMC@NLO calculation. The $\mathcal{C}^{\gamma}_{\text{data/sim}}$ factors are corrections to the simulation that account for efficiency differences in photon reconstruction with respect to data.

The ρ factor in Eq. (1) is determined from $Z \to \ell^+\ell^-$ data and is used to account for potential differences between simulation and data in the $\mathcal{R}_{Z\to\nu\overline{\nu}/\gamma}$ ratio, such as those that might be

present because of missing higher-order corrections in the simulated γ+jets term. It is given by:

$$\rho = \frac{\mathcal{R}^{\text{obs}}_{\text{Z}\to\ell^+\ell^-/\gamma}}{\mathcal{R}^{\text{sim}}_{\text{Z}\to\ell^+\ell^-/\gamma}} = \frac{N^{\text{obs}}_{\text{Z}\to\ell^+\ell^-}}{N^{\text{sim}}_{\text{Z}\to\ell^+\ell^-}} \frac{N^{\text{sim}}_{\gamma}}{N^{\text{obs}}_{\gamma}} \frac{\beta^{\text{data}}_{\ell\ell}}{\mathcal{C}^{\ell\ell}_{\text{data/sim}}} \frac{\mathcal{C}^{\gamma}_{\text{data/sim}}}{\mathcal{F}_{\text{dir}}\beta_{\gamma}}, \tag{2}$$

with $N^{\text{obs}}_{\text{Z}\to\ell^+\ell^-}$, $N^{\text{sim}}_{\text{Z}\to\ell^+\ell^-}$, and N^{sim}_{γ} the numbers of events in the indicated CRs, with the simulated samples normalized to the integrated luminosity of the data. The $\beta^{\text{data}}_{\ell\ell}$ factors represent the purity of the $\text{Z}\to\ell^+\ell^-$ CR, obtained from fits to the measured lepton-pair mass distributions, while $\mathcal{C}^{\ell\ell}_{\text{data/sim}}$ are corrections to account for data-versus-simulation differences in lepton reconstruction efficiencies. While the $\text{Z}\to\ell^+\ell^-$ sample is too small to allow a meaningful measurement of ρ in each search region, we examine the projections of ρ in each dimension. We find a modest dependence on H_{T} and on the correlated variable N_{jet}. Based on the observed empirical result $\rho(H_{\text{T}}) = 0.91 + 9.6\times10^{-5}\min(H_{\text{T}}, 900\,\text{GeV})$, we apply a weight to each simulated γ+jets event entering the evaluation of ρ and $\mathcal{R}_{\text{Z}\to\nu\bar{\nu}/\gamma}$. Following this weighting, the projections of ρ in the N_{jet}, H_{T}, and $H^{\text{miss}}_{\text{T}}$ dimensions are consistent with a constant value of 1.00, with uncertainties deduced from linear fits to the projections that vary with these variables between 2 and 13%.

For search regions with $N_{\text{b-jet}} > 0$, the $\text{Z}\to\nu\bar{\nu}$ background estimate is:

$$\left(N^{\text{pred}}_{\text{Z}\to\nu\bar{\nu}}\right)_{j,b,k} = \left(N^{\text{pred}}_{\text{Z}\to\nu\bar{\nu}}\right)_{j,0,k} \mathcal{F}_{j,b}, \tag{3}$$

where j, b, and k are bin indices (numbered from zero) for the N_{jet}, $N_{\text{b-jet}}$, and kinematic (i.e., H_{T} and $H^{\text{miss}}_{\text{T}}$) variables, respectively. For example, $j = 1$ corresponds to $N_{\text{jet}} = 3$–4, $b = 3$ to $N_{\text{b-jet}} \geq 3$, and $k = 0$ to kinematic interval 1 of Table 1 and Fig. 2. The first term on the right side of Eq. (3) is obtained from Eq. (1).

For all but the $N_{\text{jet}} \geq 9$ bin, corresponding to $j = 4$, the $N_{\text{b-jet}}$ extrapolation factor $\mathcal{F}_{j,b}$ is obtained from the fitted $\text{Z}\to\ell^+\ell^-$ data yields, with data-derived corrections $\beta^{\text{data}}_{\ell\ell}$ to account for the $N_{\text{b-jet}}$-dependent purity. Other efficiencies cancel in the ratio. Specifically,

$$\mathcal{F}_{j,b} = \left(N^{\text{data}}_{\text{Z}\to\ell^+\ell^-}\beta^{\text{data}}_{\ell\ell}\right)_{j,b} \Big/ \left(N^{\text{data}}_{\text{Z}\to\ell^+\ell^-}\beta^{\text{data}}_{\ell\ell}\right)_{j,0}; \;\; j = 0,1,2,3. \tag{4}$$

For $N_{\text{jet}} \geq 9$, there are very few $\text{Z}\to\ell^+\ell^-$ events and we use the measured results for $N_{\text{jet}} = 7-8$ (the $j = 3$ bin) multiplied by an $N_{\text{b-jet}}$ extrapolation factor from simulation:

$$\mathcal{F}_{4,b} = \mathcal{F}_{3,b}\left(N^{\text{sim}}_{\text{Z}\to\ell^+\ell^-}\right)_{4,b} / \left(N^{\text{sim}}_{\text{Z}\to\ell^+\ell^-}\right)_{3,b}. \tag{5}$$

A systematic uncertainty is assigned to the ratio of simulated yields in Eq. (5) based on a lower bound equal to 1.0 and an upper bound determined using the binomial model of Ref. [16]. The resulting uncertainty ranges from 7 to 40%, depending on $N_{\text{b-jet}}$.

A closure test of the method is presented in Fig. 4. The shaded bands represent systematic uncertainties of 7, 10, and 20% for $N_{\text{b-jet}} = 1$, 2, and ≥ 3, respectively, combined with the statistical uncertainties from the simulation. The systematic uncertainties account for the assumption that the $\mathcal{F}_{j,b}$ terms are independent of H_{T} and $H^{\text{miss}}_{\text{T}}$.

Rare processes such as $\text{t}\bar{\text{t}}\text{Z}$ and V(V)Z (V = W or Z) production can contribute to the background. We add the expectations for these processes, obtained from simulation, to the numerator and denominator of Eq. (5). Note that processes with a Z boson and a $\text{Z}\to\gamma$ counterpart are already accounted for in N^{obs}_{γ} and largely cancel in the $\mathcal{R}_{\text{Z}\to\nu\bar{\nu}/\gamma}$ ratio. For search regions

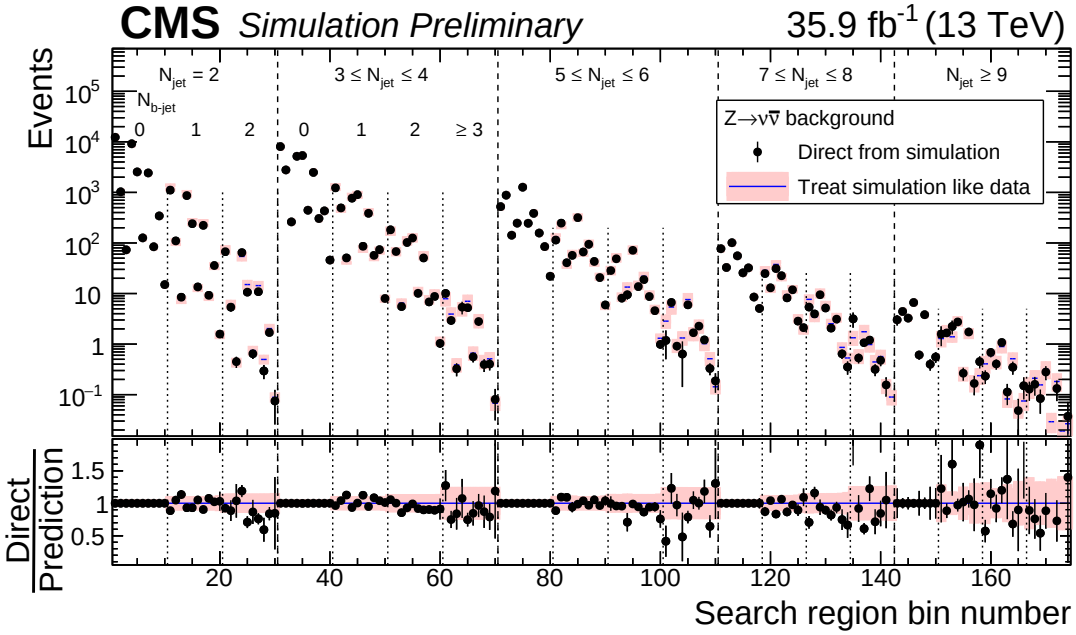

Figure 4: The $Z \to \nu\bar{\nu}$ background in the 174 search regions of the analysis as determined directly from $Z(\to \nu\bar{\nu})$+jets simulation (points), and as predicted by applying the $Z \to \nu\bar{\nu}$ background determination procedure to statistically independent $Z(\to \ell^+\ell^-)$+jets simulated event samples (histogram). For bins corresponding to $N_{\text{b-jet}} = 0$, the agreement is exact by construction. The lower panel shows the ratio between the true and predicted yields. For both the upper and lower panels, the shaded regions indicate the quadrature sum of the systematic uncertainty associated with the assumption that $\mathcal{F}_{j,b}$ is independent of H_{T} and $H_{\text{T}}^{\text{miss}}$, and the statistical uncertainty of the simulated sample. The labeling of the search regions is the same as in Fig. 3.

with $N_{\text{jet}} \geq 9$ and $N_{\text{b-jet}} \geq 2$, the contribution of $\text{t}\bar{\text{t}}\text{Z}$ events is comparable to that from Z+jets events, with an uncertainty of ≈50%, consistent with the rate and uncertainty for $\text{t}\bar{\text{t}}\text{Z}$ events found in Ref. [75].

Besides the uncertainties associated with the $N_{\text{b-jet}}$ extrapolation and the ρ term, discussed above, systematic uncertainties associated with the statistical precision of the simulation, the photon reconstruction efficiency, the photon and dilepton purities, and the $\mathcal{R}^{\text{sim}}_{Z\to\nu\bar{\nu}/\gamma}$ term are evaluated. The principal source of uncertainty arises from the limited number of events in the CRs.

7.3 Background from QCD events

Background from QCD events is not, in general, expected to be large. Nonetheless, since $H_{\text{T}}^{\text{miss}}$ in these events primarily arises from the misreconstruction of jet p_{T} rather than from genuine missing transverse momentum, it represents a difficult background to model. We employ two methods, complementary to each other, to evaluate the QCD background: the rebalance and smear (R&S) method [20, 21] and the low-$\Delta\phi$ extrapolation method [16, 76]. The R&S method is selected as our primary technique because it is more strongly motivated from first principles and is less empirical in nature. Thus the R&S method is used for the interpretation of our data, presented in Section 8. The low-$\Delta\phi$ extrapolation method is used as a cross check.

7.3.1 The rebalance and smear method

The R&S method utilizes a special CR event sample, selected using triggers that require H_T to exceed thresholds ranging from 250 to 800 GeV.

In a first step, called "rebalance," the jet momenta in a CR event are rescaled to effectively undo the effects of detector response. This step is performed using Bayesian inference. The prior probability distribution π is derived from the particle-level QCD simulation, where "particle level" corresponds to the level of an event generator, i.e., without simulation of the detector. It is given by

$$\pi(\vec{H}_T^{\text{miss}}, \vec{p}_{T,j_1}) = \mathcal{P}\left(H_T^{\text{miss}}\right)\ \mathcal{P}\left(\Delta\phi_{H_T^{\text{miss}},j_{1(b)}}\right) \tag{6}$$

where $\mathcal{P}(H_T^{\text{miss}})$ is the distribution of H_T^{miss}, and $\mathcal{P}(\Delta\phi_{H_T^{\text{miss}},j_{1(b)}})$ the distribution of the azimuthal angle between $\vec{H}_T^{\text{miss}}$ and the highest-p_T jet in the event, or between $\vec{H}_T^{\text{miss}}$ and the highest-p_T tagged b jet if $N_{\text{b-jet}} \geq 1$. The prior is binned in intervals of H_T and $N_{\text{b-jet}}$. The prior thus incorporates information about both the magnitude and direction of the genuine $\vec{H}_T^{\text{miss}}$ expected in QCD events. This represents a more sophisticated treatment than in Refs. [20, 21], where the prior was merely taken to be a Dirac delta function at $H_T^{\text{miss}} = 0$.

The jets in a CR event are then rescaled, using Bayes' theorem, to represent the event at the particle level. Jets with $p_T > 15$ GeV and $|\eta| < 5.0$ are included in this procedure. The expression of Bayes' theorem is:

$$\mathcal{P}(\vec{J}_{\text{part}}|\vec{J}_{\text{meas}}) \sim \mathcal{P}(\vec{J}_{\text{meas}}|\vec{J}_{\text{part}})\ \pi(\vec{H}_T^{\text{miss}}, \vec{p}_{T,j_1}). \tag{7}$$

The $\mathcal{P}(\vec{J}_{\text{part}}|\vec{J}_{\text{meas}})$ term is the posterior probability density, expressing the probability for a given set of particle-level jet momenta $\vec{J}_{\text{part}}$ given the measured set $\vec{J}_{\text{meas}}$. The $\mathcal{P}(\vec{J}_{\text{meas}}|\vec{J}_{\text{part}})$ term is a likelihood function, defined by the product over the jets in the event of the response functions for the individual jets. The jet response functions, determined in bins of jet p_T and η, are derived from simulation as the distribution of the ratio of reconstructed jet p_T values for a given generated value, corrected with separate scale factors for the Gaussian cores and non-Gaussian tails to account for jet energy resolution differences with respect to data. The likelihood function is maximized by rescaling the momenta of the measured jets, with the respective jet p_T uncertainties as constraints. The set $\vec{J}_{\text{part}}$ corresponding to the resulting most-likely posterior probability defines the rebalanced event.

In a second step, denoted "smear," the magnitudes of the jet momenta are rescaled by p_T- and η-dependent factors obtained from random sampling of the jet response functions. This sampling is performed numerous times for each rebalanced event to increase the statistical precision of the resulting sample.

Application of the R&S procedure produces an event sample that closely resembles the original sample of CR events, except the contributions of events with genuine H_T^{miss}, viz., top quark, W+jets, Z+jets, and possible signal events, are effectively eliminated [20]. The rebalanced and smeared events are subjected to the standard event selection criteria of Section 4 to obtain the predictions for the QCD background in each search region.

The principal uncertainty in the R&S QCD background prediction is systematic, associated with the uncertainty in the shape of the jet response functions. This uncertainty is evaluated by varying the jet energy resolution scale factors within their uncertainties, resulting in uncertainties in the prediction that range from 20–80% depending on the search region. Smaller uncertainties related to the trigger, the prior, and the statistical terms are also evaluated.

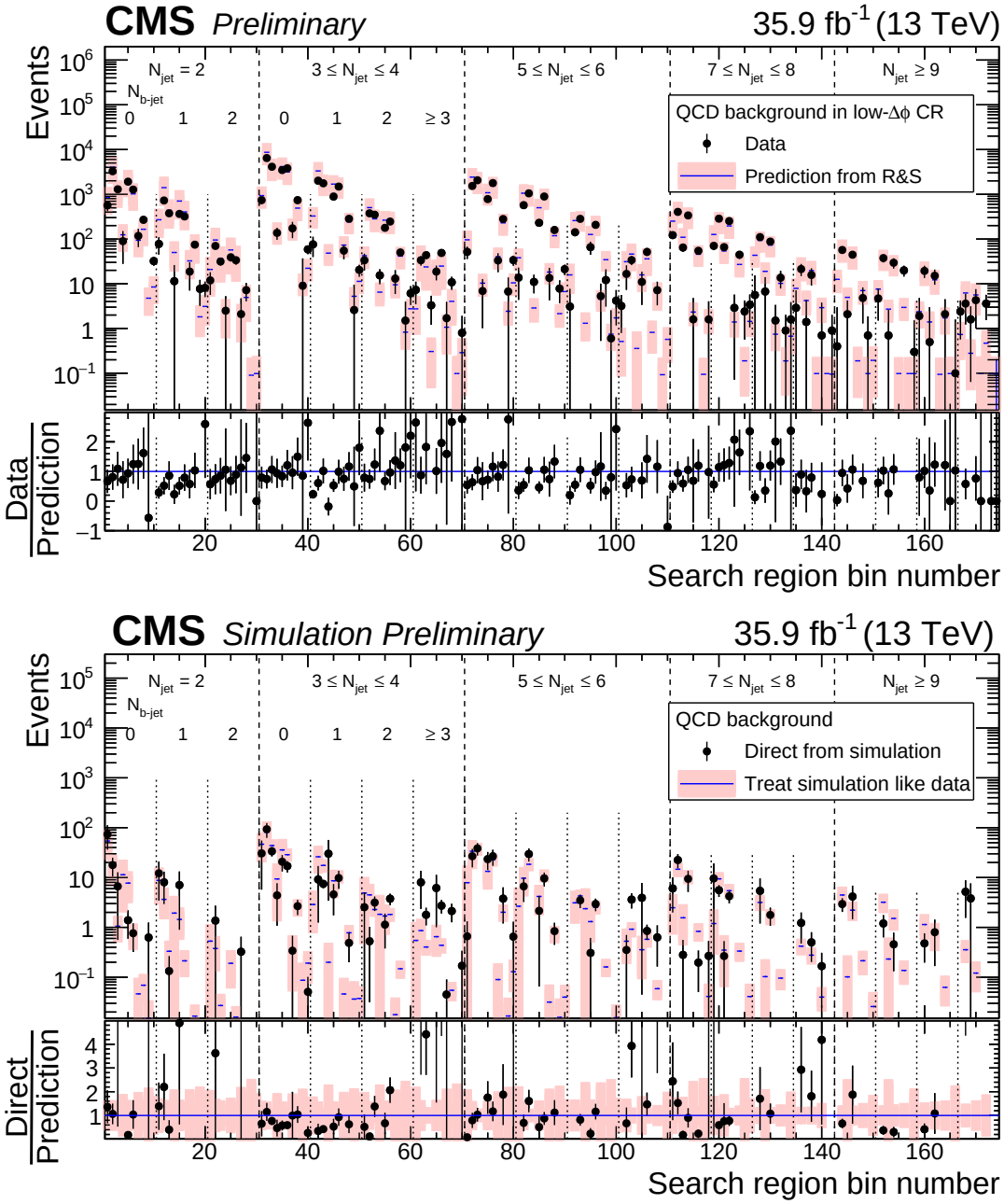

Figure 5: (Upper plot) The QCD background in the low-$\Delta\phi$ control region (CR) as predicted by the rebalance and smear (R&S) method (histograms, with statistical and systematic uncertainties added in quadrature), compared to the corresponding data from which the expected contributions of top quark, W+jets, and Z+jets events have been subtracted (points, with statistical uncertainties). The lower panel shows the ratio of the measured to the predicted results. (Lower plot) The QCD background in the 174 search regions of the analysis as determined directly from QCD simulation (points, with statistical uncertainties) and as predicted by applying the low-$\Delta\phi$ extrapolation QCD background determination procedure to simulated event samples (histograms, with statistical and systematic uncertainties added in quadrature). The lower panel shows the same results following division by the predicted value. Bins without markers have no events in the control regions. No result is given in the lower panel if the value of the prediction is zero. For both the upper and lower plots, the labeling of the search regions is the same as in Fig. 3.

As a test of the method, we determine the R&S prediction for the QCD contribution to a QCD-dominated CR selected with the standard trigger and event selection, except for the $\Delta\phi_{H_{\mathrm{T}}^{\mathrm{miss}},j_{\mathrm{i}}}$ requirements of Section 4, which are inverted. Specifically, at least one of the two (for $N_{\mathrm{jet}} = 2$), three (for $N_{\mathrm{jet}} = 3$), or four (for $N_{\mathrm{jet}} \geq 4$) highest p_{T} jets in an event must fail a $\Delta\phi_{H_{\mathrm{T}}^{\mathrm{miss}},j_{\mathrm{i}}}$ selection criterion. The resulting QCD-dominated sample is called the low-$\Delta\phi$ CR. The R&S prediction for the QCD background in the low-$\Delta\phi$ CR is shown in Fig. 5 (upper plot) in comparison to the corresponding measured results, following subtraction from the data of the contributions from top quark, W+jets, and Z+jets events, evaluated as described in the previous sections. The prediction from the R&S method is seen to agree with the data within the uncertainties.

7.3.2 The low-$\Delta\phi$ extrapolation method

In the low-$\Delta\phi$ extrapolation method, the QCD background in each search region is evaluated by multiplying the observed event yield in the corresponding region of the low-$\Delta\phi$ CR (Section 7.3.1), after accounting for the contributions of non-QCD SM events, by a factor R^{QCD} determined primarily from data. The R^{QCD} terms express the ratio of the expected QCD background in the corresponding signal and low-$\Delta\phi$ regions.

The R^{QCD} term is empirically observed to have a negligible dependence on $N_{\text{b-jet}}$ for a given value of N_{jet}. The functional dependence of R^{QCD} can therefore be expressed in terms of H_{T}, $H_{\mathrm{T}}^{\mathrm{miss}}$, and N_{jet} alone. The R^{QCD} term is modeled as:

$$R^{\mathrm{QCD}}_{i,j,k} = K^{\mathrm{data}}_{ij}\, S^{\mathrm{sim}}_{ik}\,, \tag{8}$$

with i, j, and k the H_{T}, N_{jet}, and $H_{\mathrm{T}}^{\mathrm{miss}}$ bin indices, respectively. In Ref. [16] we used a model in which the H_{T}, $H_{\mathrm{T}}^{\mathrm{miss}}$, and N_{jet} dependencies in R^{QCD} factorized. For the $N_{\mathrm{jet}} = 2$ search regions, introduced for the present study, this factorization is found to be less well justified and we adopt the parameterization of Eq. (8).

The K^{data}_{ij} factors are determined from a maximum likelihood fit to data in a sideband region defined by $250 < H_{\mathrm{T}}^{\mathrm{miss}} < 300\,\mathrm{GeV}$ (regions C1, C2, and C3 in Fig. 2). They are the ratio of the number of QCD events in the high-$\Delta\phi$ region to that in the low-$\Delta\phi$ region, where "high $\Delta\phi$" refers to events selected with the standard (non-inverted) $\Delta\phi_{H_{\mathrm{T}}^{\mathrm{miss}},j_{\mathrm{i}}}$ requirements. The fit accounts for the contributions of top quark, W+jets, and Z+jets events using the techniques described in the preceding sections. Uncertainties in K^{data}_{ij} are determined from the covariance matrix of the fit. The S^{sim}_{ik} terms, taken from the QCD simulation, represent corrections to account for the $H_{\mathrm{T}}^{\mathrm{miss}}$ dependence of R^{QCD}. Based on studies of the differing contributions of events in which the jet with the largest p_{T} mismeasurement is or is not amongst the two (for $N_{\mathrm{jet}} = 2$), three (for $N_{\mathrm{jet}} = 3$), or four (for $N_{\mathrm{jet}} \geq 4$) highest p_{T} jets, uncertainties between 14 and 100% are assigned to the S^{sim}_{ik} terms to account for potential differences between data and simulation. The total uncertainties in S^{sim}_{ik} are defined by the sum in quadrature of the systematic uncertainties and the statistical uncertainties from the simulation.

Figure 5 (lower plot) presents a closure test for the method. An additional systematic uncertainty is included in R^{QCD} to account for the level of nonclosure. Figure 6 shows a comparison between the predictions of the R&S and $\Delta\phi$ methods, which are seen to agree.

8 Results

Figure 7 presents the observed numbers of events in the 174 search regions. The data are shown in comparison with the summed predictions for the SM backgrounds. Numerical values are

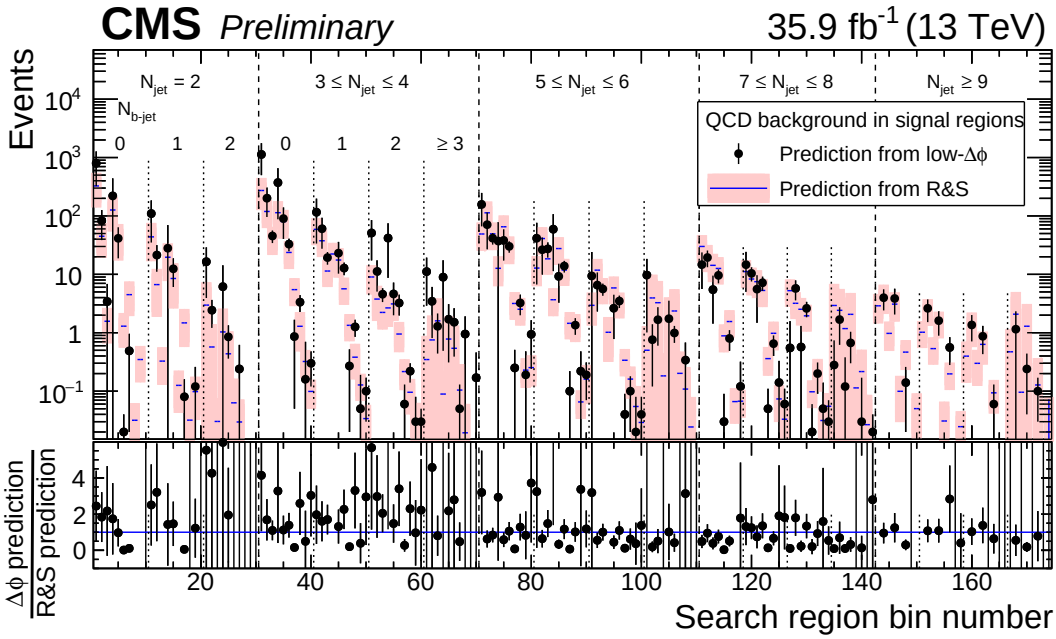

Figure 6: Comparison between the predictions for the number of QCD events in the 174 search regions of the analysis as determined from the rebalance and smear (R&S, histograms) and low-$\Delta\phi$ extrapolation (points) methods. For both methods, the error bars indicate the combined statistical and systematic uncertainties. The lower panel shows the ratio of the low-$\Delta\phi$ extrapolation to the R&S results. The labeling of the search regions is the same as in Fig. 3.

given in Tables B.1–B.5 of Appendix B. The evaluated SM background is found to be statistically consistent with the data in all 174 regions. Thus, we do not obtain evidence for supersymmetry.

In addition to the finely segmented search regions of Fig. 7, we evaluate the background predictions in 12 aggregate regions, determined by summing the results from the nominal search regions while accounting for correlations. The aggregate regions are intended to represent 12 potentially interesting signal topologies. While the aggregate regions do not provide as much sensitivity to the presence of new physics as the full set of search regions, they allow our data to be used in a simpler manner for the investigation of signal scenarios not examined in this note. The aggregate regions, and the signal topologies they are intended to help probe, are specified in Table 3. The first 10 regions are characterized by their heavy flavor (top or bottom quark) content, parton multiplicity, and the mass difference Δm discussed in Section 6. The last two regions target models with direct top squark production. The results for the aggregate regions are presented in Fig. 8, with numerical values provided in Table B.6 of Appendix B.

In Fig. 9, we present one-dimensional projections of the data and SM predictions in either the $H_{\mathrm{T}}^{\mathrm{miss}}$, N_{jet}, or $N_{\text{b-jet}}$ variable after imposing criteria, indicated in the legends, to enhance the expected contributions of T1tttt, T1bbbb, T1qqqq, T2tt, T2bb, or T2qq events. In each case, two example signal distributions are shown: one with $\Delta m \gg 0$, and one with $\Delta m \approx 0$, where both example scenarios lie well within the parameter space excluded by the present study.

Limits are evaluated for the production cross sections of the signal scenarios using a likelihood fit, with the SUSY signal strength, the yields of the four classes of background shown in Fig. 7, and various nuisance parameters as fitted parameters, where a nuisance parameter refers to a variable of little physical interest, such as a scale factor in a background determination procedure. For the models of gluino (squark) pair production, the limits are derived as a function of $m_{\tilde{\mathrm{g}}}$ ($m_{\tilde{\mathrm{q}}}$) and $m_{\tilde{\chi}_1^0}$. The likelihood function is given by the product of Poisson probability density

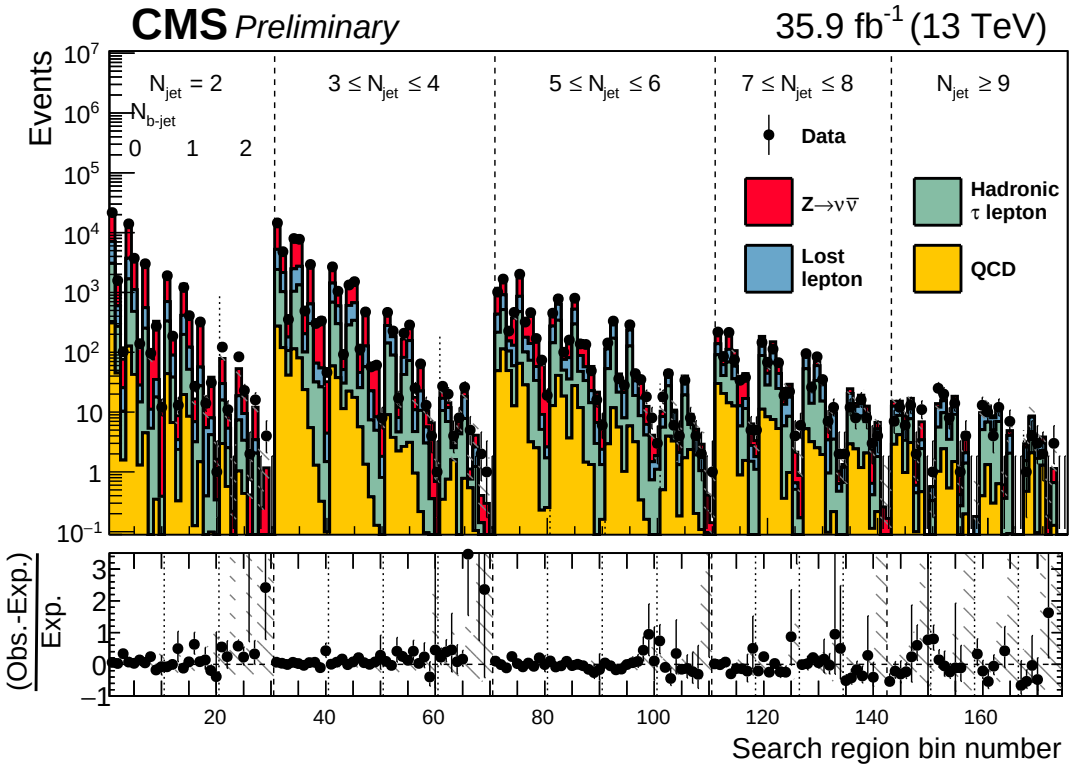

Figure 7: The observed numbers of events and prefit SM background predictions in the 174 search regions of the analysis. Numerical values are given in Tables B.1–B.5. The hatching indicates the total uncertainties in the background predictions. The lower panel displays the fractional differences between the data and SM predictions. The labeling of the search regions is the same as in Fig. 3.

functions, one for each search region, and constraints that account for uncertainties in the background predictions and signal yields. These uncertainties are treated as nuisance parameters with log-normal probability density functions. Correlations are taken into account. The signal yield uncertainties associated with the renormalization and factorization scales, ISR, jet energy scale, b jet tagging, pileup, and statistical fluctuations are evaluated as a function of $m_{\tilde{g}}$ and $m_{\tilde{\chi}_1^0}$, or $m_{\tilde{q}}$ and $m_{\tilde{\chi}_1^0}$. The test statistic is $q_\mu = -2\ln\left(\mathcal{L}_\mu/\mathcal{L}_{\text{max}}\right)$, where $\mathcal{L}_{\text{max}}$ is the maximum likelihood determined by allowing all parameters including the SUSY signal strength μ to vary, and $\mathcal{L}_\mu$ is the maximum likelihood for a fixed signal strength. To set limits, asymptotic results for the test statistic [77] are used, in conjunction with the CL_s criterion described in Refs. [78, 79].

We evaluate 95% confidence level (CL) upper limits on the signal cross sections. The NLO+NLL cross section is used to determine corresponding 95% CL exclusion curves. Beyond the observed exclusion limits, we derive expected exclusion limits by using the expected Poisson fluctuations around the predicted numbers of background events when evaluating the test statistic. Signal contamination is taken into account by considering the expected contribution to the CRs of the signal model being examined, and adjusting the signal region background predictions accordingly when deriving the limits for that signal model.

The results for the T1tttt, T1bbbb, T1qqqq, and T5qqqqVV models are shown in the upper and middle rows of Fig. 10. Depending on the value of $m_{\tilde{\chi}_1^0}$, and using the NLO+NLL cross sections, gluinos with masses as large as 1970, 1950, 1840, and 1800 GeV, respectively, are excluded. These results significantly extend those of our previous study [16], for which the corresponding

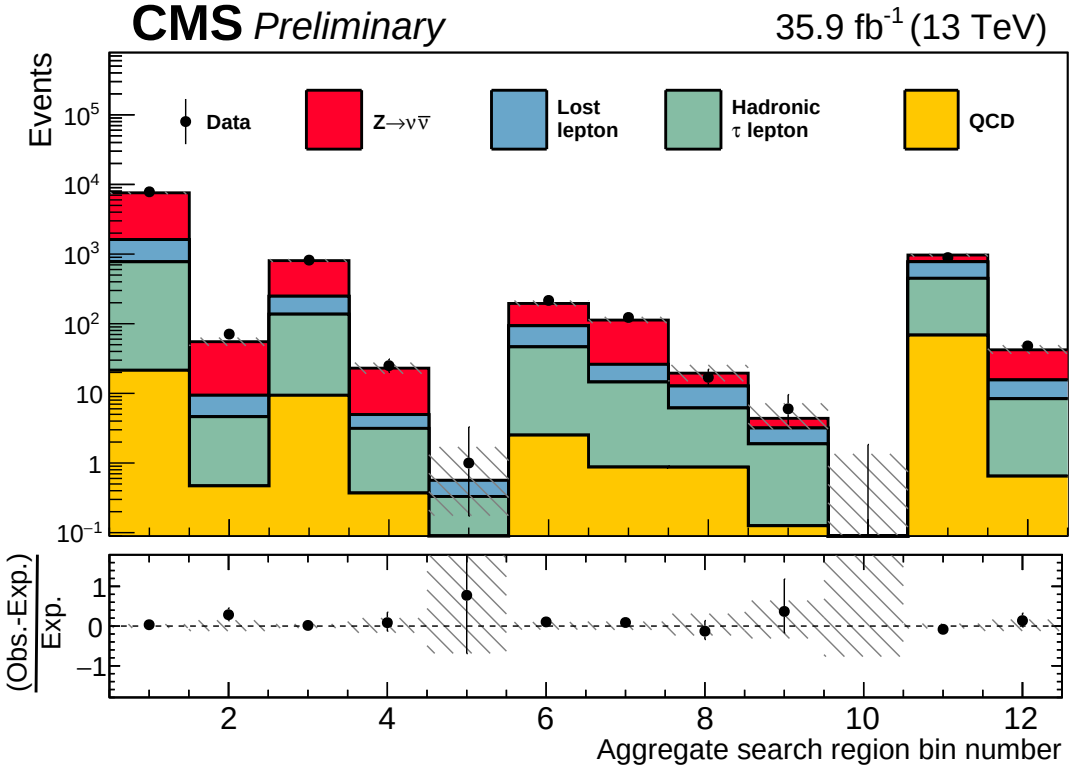

Figure 8: The observed numbers of events and prefit SM background predictions in the 12 aggregate search regions, with fractional differences displayed in the lower panel. The hatching indicates the total uncertainties in the background predictions. The numerical values are given in Table B.6.

Table 3: Definition of the aggregate search regions.

Region	Heavy flavor?	Parton multiplicity	Δm	N_{jet}	$N_{\text{b-jet}}$	H_{T} [GeV]	$H_{\text{T}}^{\text{miss}}$ [GeV]
1	No	Low	Small	≥ 2	0	≥ 500	≥ 500
2	No	Low	Large	≥ 3	0	≥ 1500	≥ 750
3	No	Medium	Small	≥ 5	0	≥ 500	≥ 500
4	No	Medium	Large	≥ 5	0	≥ 1500	≥ 750
5	No	High	All	≥ 9	0	≥ 1500	≥ 750
6	Yes	Low	Small	≥ 2	≥ 2	≥ 500	≥ 500
7	Yes	Low	Large	≥ 3	≥ 1	≥ 750	≥ 750
8	Yes	Medium	Small	≥ 5	≥ 3	≥ 500	≥ 500
9	Yes	Medium	Large	≥ 5	≥ 2	≥ 1500	≥ 750
10	Yes	High	All	≥ 9	≥ 3	≥ 750	≥ 750
11		$\widetilde{\text{t}}$-like	Small	≥ 7	≥ 1	≥ 300	≥ 300
12		$\widetilde{\text{t}}$-like	Large	≥ 5	≥ 1	≥ 750	≥ 750

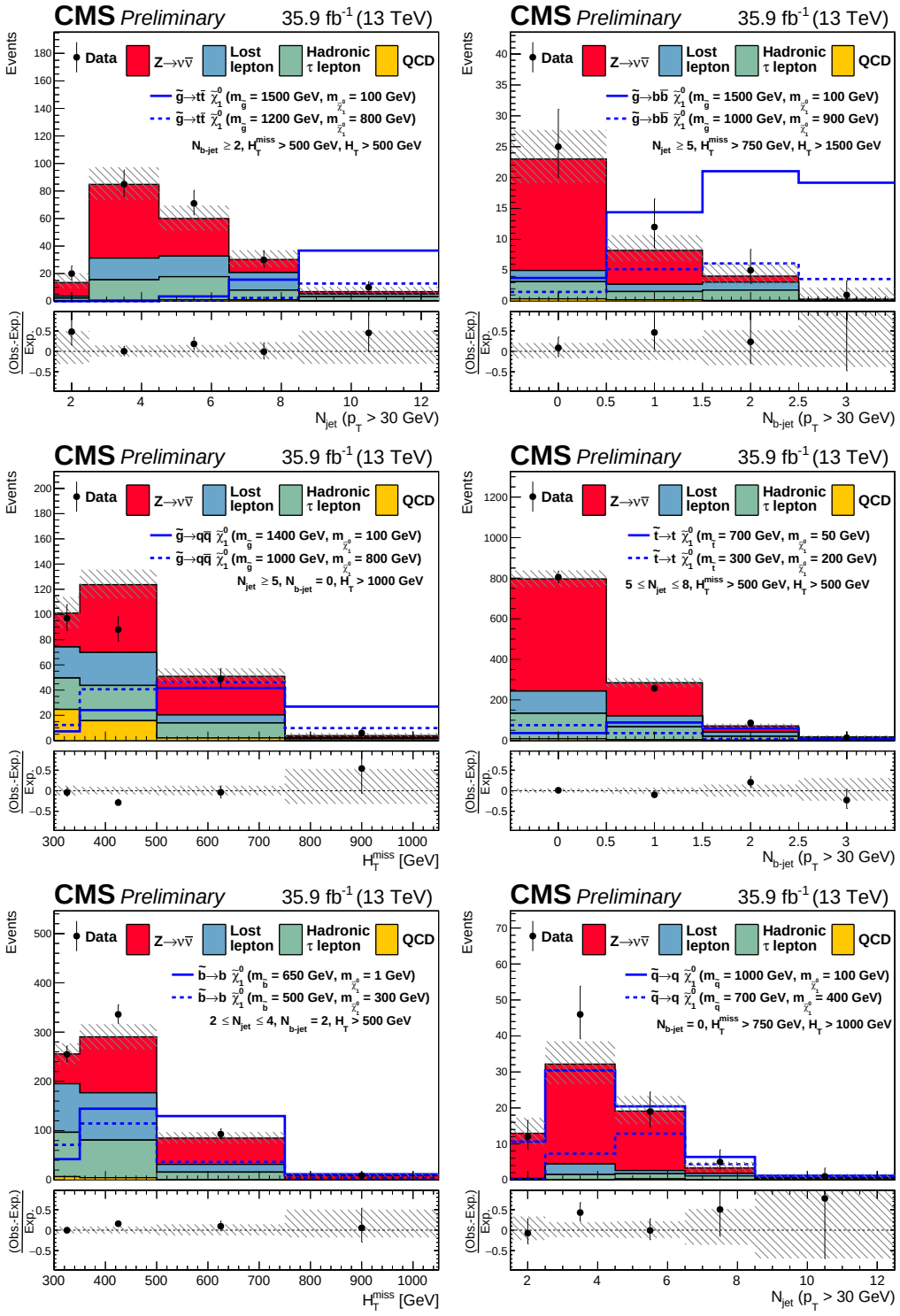

Figure 9: The observed numbers of events and SM background predictions for regions in the search region parameter space particularly sensitive to the production of events in the (upper left) T1tttt, (upper right) T1bbbb, (middle left) T1qqqq, (middle right) T2tt, (lower left) T2bb, and (lower right) T2qq scenarios. The selection requirements are given in the figure legends. The hatched regions indicate the total uncertainties in the background predictions. The (unstacked) results for two example signal scenarios are shown in each instance, one with $\Delta m \gg 0$ and the other with $\Delta m \approx 0$, where Δm is the difference between the gluino or squark mass and the sum of the masses of the particles into which it decays.

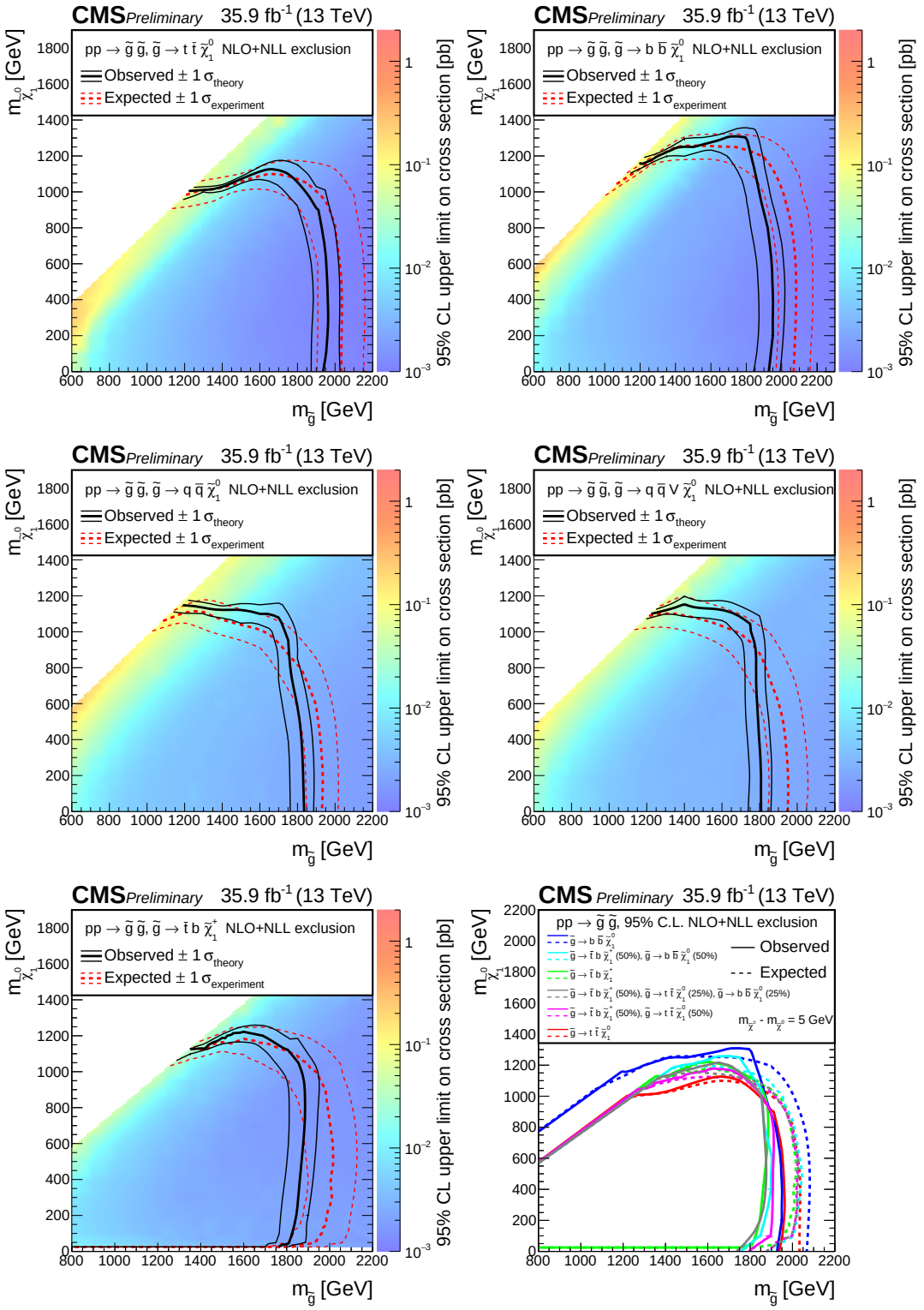

Figure 10: The 95% CL upper limits on the production cross sections for the (upper left) T1tttt, (upper right) T1bbbb, (middle left) T1qqqq, (middle right) T5qqqqVV, and (lower left) T1tbtb simplified models, shown as a function of the gluino and LSP masses $m_{\tilde{g}}$ and $m_{\tilde{\chi}_1^0}$. The solid (black) curves show the observed exclusion contours assuming the NLO+NLL cross sections [61–65], with the corresponding ± 1 standard deviation uncertainties [80]. The dashed (red) curves present the expected limits with ± 1 standard deviation experimental uncertainties. (Lower right) The corresponding 95% NLO+NLL exclusion curves for the mixed models of gluino decays to heavy squarks. For the T1tbtb model, the results are restricted to $m_{\tilde{\chi}_1^0} > 25\,\text{GeV}$ for the reason stated in the text.

limits vary between 1440 and 1600 GeV.

The corresponding results for the T1tbtb model and for the mixed models of gluino decay to heavy squarks are shown in the lower row of Fig. 10. In this case gluinos with masses as large as 1880 to 1910 GeV are excluded, extending the limits of between 1550 and 1600 GeV presented in Ref. [18]. Note that for the T1tbtb model, the acceptance is small for $m_{\widetilde{\chi}_1^0} \lesssim 25\,\text{GeV}$ and we are unable to exclude the scenario. The reason is that as $m_{\widetilde{\chi}_1^0}$ approaches zero, the mass of the nearly mass-degenerate $\widetilde{\chi}_1^\pm$ parent particle also becomes small. The $\widetilde{\chi}_1^\pm$ becomes highly Lorentz boosted, and more of the momentum from the parent $\widetilde{\chi}_1^\pm$ is carried by the daughter virtual W boson [see Fig. 1 (upper right)] and less by the daughter $\widetilde{\chi}_1^0$ LSP. The net effect is that the H_T^miss spectrum becomes softer for hadronic W^* decays, leading to reduced signal acceptance, while the charged lepton or isolated-track p_T spectrum becomes harder for leptonic W^* decays, increasing the probability for the event to be vetoed and thus also leading to reduced signal acceptance. Furthermore, jets arising from the W^* decay tend to be aligned with the missing transverse momentum from the $\widetilde{\chi}_1^0$. When these jets become harder, as $m_{\widetilde{\chi}_1^0}$ becomes small, they are more likely to appear amongst the highest p_T jets in the event, causing the event to be rejected by the $\Delta\phi_{H_\text{T}^\text{miss},j_i}$ requirements. Because of the small signal acceptance for $m_{\widetilde{\chi}_1^0} \to 0$, the relative contribution of signal contamination in this region becomes comparable to the true signal content, and a precise determination of the search sensitivity becomes difficult. Therefore, for the T1tbtb model, we limit our determination of the cross section upper limit to $m_{\widetilde{\chi}_1^0} > 25\,\text{GeV}$.

Finally, Fig. 11 shows the results for the T2tt, T2bb, and T2qq models. Based on the NLO+NLL cross sections, squarks with masses up to 970, 1040, and 1450 GeV, respectively, are excluded. Note that for the T2tt model we do not present cross section upper limits for small values of $m_{\widetilde{\chi}_1^0}$ if $m_{\widetilde{\text{q}}} - m_{\widetilde{\chi}_1^0} \approx m_\text{top}$, corresponding to the unshaded diagonal region at low $m_{\widetilde{\chi}_1^0}$ visible in Fig. 11 (upper left). The reason for this is that signal events are essentially indistinguishable from SM $\text{t}\bar{\text{t}}$ events in this region, rendering the signal event acceptance difficult to model.

In addition to the main T2qq model, with four mass-degenerate squark flavors (up, down, strange, and charm), each arising from two different quark spin states, Fig. 11 (lower) shows the results should only one of these eight states ("one light $\widetilde{\text{q}}$") be accessible at the LHC. In this case, the upper limit on the squark mass based on the NLO+NLL cross section is reduced to 1050 GeV.

9 Summary

A search for gluino and squark pair production is presented based on a sample of proton-proton collisions collected at center-of-mass energy $\sqrt{s} = 13\,\text{TeV}$ with the CMS detector. The search is performed in the multijet channel, i.e., the visible reconstructed final state consists solely of jets. The data correspond to an integrated luminosity of $35.9\,\text{fb}^{-1}$. Events are required to have at least two jets, $H_\text{T} > 300\,\text{GeV}$, and $H_\text{T}^\text{miss} > 300\,\text{GeV}$, where H_T is the scalar sum of jet transverse momenta p_T. The H_T^miss variable, used as a measure of missing transverse momentum, is the magnitude of the vector p_T sum of jets. Jets are required to have $p_\text{T} > 30\,\text{GeV}$.

The data are examined in 174 exclusive four-dimensional search regions defined by the number of jets, the number of tagged bottom quark jets, H_T, and H_T^miss. Background from standard model processes is evaluated using control samples in the data. We also provide results for 12 aggregated search regions, to simplify use of our data by others. The estimates of the standard model background are found to agree with the observed numbers of events for all regions.

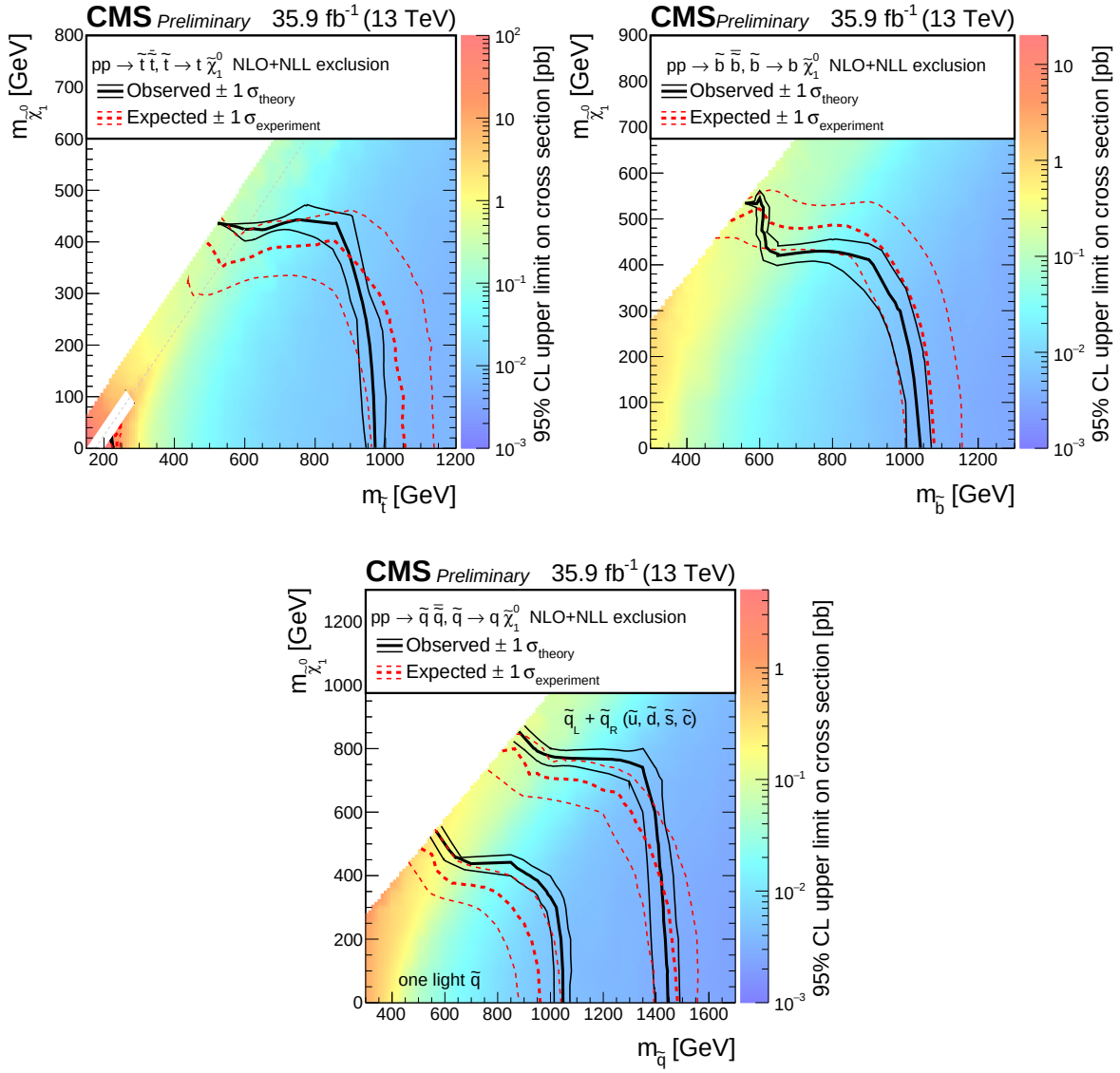

Figure 11: (Left) The 95% CL upper limits on the production cross section for the (upper left) T2tt, (upper right) T2bb, and (lower) T2qq simplified models, shown as a function of the squark and LSP masses $m_{\tilde{q}}$ and $m_{\tilde{\chi}_1^0}$. The diagonal dotted line shown for the T2tt model corresponds to $m_{\tilde{q}} - m_{\tilde{\chi}_1^0} = m_{\text{top}}$. The results labeled "one light $\tilde{q}$" for the T2qq model are discussed in the text. The meaning of the curves is described in the Fig. 10 caption.

The results are interpreted in the context of simplified models. We consider models in which pair-produced gluinos each decay to a $t\bar{t}$ pair and an undetected, stable, lightest-supersymmetric-particle neutralino $\widetilde{\chi}_1^0$ (T1tttt model); to a $b\bar{b}$ pair and the $\widetilde{\chi}_1^0$ (T1bbbb model); to a light-flavored $q\bar{q}$ pair and the $\widetilde{\chi}_1^0$ (T1qqqq model); to a light-flavored quark and antiquark and either the second-lightest neutralino $\widetilde{\chi}_2^0$ or the lightest chargino $\widetilde{\chi}_1^\pm$, followed by decay of the $\widetilde{\chi}_2^0$ ($\widetilde{\chi}_1^\pm$) to the $\widetilde{\chi}_1^0$ and an on- or off-shell Z ($W^\pm$) boson (T5qqqqVV model); or to $\bar{t}b\widetilde{\chi}_1^+$ or $t\bar{b}\widetilde{\chi}_1^-$, followed by the decay of the $\widetilde{\chi}_1^\pm$ to the $\widetilde{\chi}_1^0$ and an off-shell W boson (T1tbtb model). To provide more model independence, we also consider mixed scenarios in which a gluino can decay to $t\bar{t}\widetilde{\chi}_1^0$, $b\bar{b}\widetilde{\chi}_1^0$, $\bar{t}b\widetilde{\chi}_1^+$, or $t\bar{b}\widetilde{\chi}_1^-$ with various probabilities. Beyond the models for gluino production, we examine models for direct squark pair production. We consider scenarios in which each squark decays to a top quark and the $\widetilde{\chi}_1^0$ (T2tt model); to a bottom quark and the $\widetilde{\chi}_1^0$ (T2bb model); or to a light-flavored (u, d, s, c) quark and the $\widetilde{\chi}_1^0$ (T2qq model).

Using the predicted cross sections with next-to-leading-order plus next-to-leading-logarithm accuracy as a reference, gluinos with masses as large as 1800 to 1970 GeV are excluded, depending on the scenario. The corresponding limits on the mass of directly produced squarks range from 970 to 1450 GeV. These results extend those from previous searches.

References

[1] R. Barbieri and G. F. Giudice, "Upper Bounds on Supersymmetric Particle Masses", *Nucl. Phys. B* **306** (1988) 63, doi:10.1016/0550-3213(88)90171-X.

[2] P. Ramond, "Dual theory for free fermions", *Phys. Rev. D* **3** (1971) 2415, doi:10.1103/PhysRevD.3.2415.

[3] Y. A. Golfand and E. P. Likhtman, "Extension of the algebra of Poincaré group generators and violation of P invariance", *JETP Lett.* **13** (1971) 323.

[4] A. Neveu and J. H. Schwarz, "Factorizable dual model of pions", *Nucl. Phys. B* **31** (1971) 86, doi:10.1016/0550-3213(71)90448-2.

[5] D. V. Volkov and V. P. Akulov, "Possible universal neutrino interaction", *JETP Lett.* **16** (1972) 438.

[6] J. Wess and B. Zumino, "A Lagrangian model invariant under supergauge transformations", *Phys. Lett. B* **49** (1974) 52, doi:10.1016/0370-2693(74)90578-4.

[7] J. Wess and B. Zumino, "Supergauge transformations in four dimensions", *Nucl. Phys. B* **70** (1974) 39, doi:10.1016/0550-3213(74)90355-1.

[8] P. Fayet, "Supergauge invariant extension of the Higgs mechanism and a model for the electron and its neutrino", *Nucl. Phys. B* **90** (1975) 104, doi:10.1016/0550-3213(75)90636-7.

[9] H. P. Nilles, "Supersymmetry, supergravity and particle physics", *Phys. Rep.* **110** (1984) 1, doi:10.1016/0370-1573(84)90008-5.

[10] S. Dimopoulos and G. F. Giudice, "Naturalness constraints in supersymmetric theories with nonuniversal soft terms", *Phys. Lett. B* **357** (1995) 573, doi:10.1016/0370-2693(95)00961-J, arXiv:hep-ph/9507282.

[11] R. Barbieri and D. Pappadopulo, "S-particles at their naturalness limits", *JHEP* **10** (2009) 061, doi:10.1088/1126-6708/2009/10/061, arXiv:0906.4546.

[12] M. Papucci, J. T. Ruderman, and A. Weiler, "Natural SUSY endures", *JHEP* **09** (2012) 035, doi:10.1007/JHEP09(2012)035, arXiv:1110.6926.

[13] G. R. Farrar and P. Fayet, "Phenomenology of the production, decay, and detection of new hadronic states associated with supersymmetry", *Phys. Lett. B* **76** (1978) 575, doi:10.1016/0370-2693(78)90858-4.

[14] ATLAS Collaboration, "Search for pair production of gluinos decaying via stop and sbottom in events with b-jets and large missing transverse momentum in pp collisions at $\sqrt{s} = 13$ TeV with the ATLAS detector", *Phys. Rev. D* **94** (2016) 032003, doi:10.1103/PhysRevD.94.032003, arXiv:1605.09318.

[15] ATLAS Collaboration, "Search for squarks and gluinos in final states with jets and missing transverse momentum at $\sqrt{s} = 13$ TeV with the ATLAS detector", *Eur. Phys. J. C* **76** (2016) 392, doi:10.1140/epjc/s10052-016-4184-8, arXiv:1605.03814.

[16] CMS Collaboration, "Search for supersymmetry in the multijet and missing transverse momentum final state in pp collisions at 13 TeV", *Phys. Lett. B* **758** (2016) 152, doi:10.1016/j.physletb.2016.05.002, arXiv:1602.06581.

[17] CMS Collaboration, "Search for new physics with the M_{T2} variable in all-jets final states produced in pp collisions at $\sqrt{s} = 13$ TeV", *JHEP* **10** (2016) 006, doi:10.1007/JHEP10(2016)006, arXiv:1603.04053.

[18] CMS Collaboration, "Inclusive search for supersymmetry using razor variables in pp collisions at $\sqrt{s} = 13$TeV", *Phys. Rev. D* **95** (2017) 012003, doi:10.1103/PhysRevD.95.012003, arXiv:1609.07658.

[19] CMS Collaboration, "A search for new phenomena in pp collisions at $\sqrt{s} = 13$ TeV in final states with missing transverse momentum and at least one jet using the α_T variable", (2016). arXiv:1611.00338. Submitted to *Eur. Phys. J. C*.

[20] CMS Collaboration, "Search for new physics with jets and missing transverse momentum in pp collisions at $\sqrt{s} = 7$ TeV", *JHEP* **08** (2011) 155, doi:10.1007/JHEP08(2011)155, arXiv:1106.4503.

[21] CMS Collaboration, "Search for new physics in the multijet and missing transverse momentum final state in proton-proton collisions at $\sqrt{s} = 8$ TeV", *JHEP* **06** (2014) 055, doi:10.1007/JHEP06(2014)055, arXiv:1402.4770.

[22] N. Arkani-Hamed et al., "MARMOSET: The path from LHC data to the new standard model via on-shell effective theories", (2007). arXiv:hep-ph/0703088.

[23] J. Alwall, P. Schuster, and N. Toro, "Simplified models for a first characterization of new physics at the LHC", *Phys. Rev. D* **79** (2009) 075020, doi:10.1103/PhysRevD.79.075020, arXiv:0810.3921.

[24] J. Alwall, M.-P. Le, M. Lisanti, and J. G. Wacker, "Model-independent jets plus missing energy searches", *Phys. Rev. D* **79** (2009) 015005, doi:10.1103/PhysRevD.79.015005, arXiv:0809.3264.

[25] D. Alves et al., "Simplified models for LHC new physics searches", *J. Phys. G* **39** (2012) 105005, doi:10.1088/0954-3899/39/10/105005, arXiv:1105.2838.

[26] CMS Collaboration, "Interpretation of searches for supersymmetry with simplified models", *Phys. Rev. D* **88** (2013) 052017, doi:10.1103/PhysRevD.88.052017, arXiv:1301.2175.

[27] CMS Collaboration, "The CMS experiment at the CERN LHC", *JINST* **3** (2008) S08004, doi:10.1088/1748-0221/3/08/S08004.

[28] CMS Collaboration, "The CMS trigger system", *JINST* **12** (2017) P01020, doi:10.1088/1748-0221/12/01/P01020, arXiv:1609.02366.

[29] CMS Collaboration, "Particle flow event reconstruction in CMS and performance for jets, taus and E_T^{miss}", CMS Physics Analysis Summary CMS-PAS-PFT-09-001, CERN, 2009.

[30] CMS Collaboration, "Commissioning of the particle-flow event reconstruction with the first LHC collisions recorded in the CMS detector", CMS Physics Analysis Summary CMS-PAS-PFT-10-001, CERN, 2010.

[31] CMS Collaboration, "Performance of electron reconstruction and selection with the CMS detector in proton-proton collisions at $\sqrt{s} = 8$ TeV", *JINST* **10** (2015) P06005, doi:10.1088/1748-0221/10/06/P06005, arXiv:1502.02701.

[32] CMS Collaboration, "The performance of the CMS muon detector in proton-proton collisions at $\sqrt{s} = 7$ TeV at the LHC", *JINST* **8** (2013) P11002, doi:10.1088/1748-0221/8/11/P11002, arXiv:1306.6905.

[33] CMS Collaboration, "Study of pileup removal algorithms for jets", CMS Physics Analysis Summary CMS-PAS-JME-14-001, CERN, 2014.

[34] K. Rehermann and B. Tweedie, "Efficient Identification of Boosted Semileptonic Top Quarks at the LHC", *JHEP* **03** (2011) 059, doi:10.1007/JHEP03(2011)059, arXiv:1007.2221.

[35] M. Cacciari, G. P. Salam, and G. Soyez, "The Anti-k_t jet clustering algorithm", *JHEP* **04** (2008) 063, doi:10.1088/1126-6708/2008/04/063, arXiv:0802.1189.

[36] M. Cacciari, G. P. Salam, and G. Soyez, "FastJet user manual", *Eur. Phys. J. C* **72** (2012) 1896, doi:10.1140/epjc/s10052-012-1896-2, arXiv:1111.6097.

[37] CMS Collaboration, "Jet performance in pp collisions at $\sqrt{s} = 7$ TeV", CMS Physics Analysis Summary CMS-PAS-JME-10-003, CERN, 2010.

[38] CMS Collaboration, "Jet energy scale and resolution in the CMS experiment in pp collisions at 8 TeV", *JINST* **12** (2017) P02014, doi:10.1088/1748-0221/12/02/P02014, arXiv:1607.03663.

[39] M. Cacciari and G. P. Salam, "Pileup subtraction using jet areas", *Phys. Lett. B* **659** (2008) 119, doi:10.1016/j.physletb.2007.09.077, arXiv:0707.1378.

[40] CMS Collaboration, "Identification of b quark jets at the CMS experiment in the LHC Run 2", CMS Physics Analysis Summary CMS-PAS-BTV-15-001, CERN, 2016.

[41] UA1 Collaboration, "Experimental Observation of Isolated Large Transverse Energy Electrons with Associated Missing Energy at $\sqrt{s} = 540$ GeV", *Phys. Lett. B* **122** (1983) 103, doi:10.1016/0370-2693(83)91177-2.

[42] CMS Collaboration, "Performance of missing energy reconstruction in 13 TeV pp collision data using the CMS detector", CMS Physics Analysis Summary CMS-PAS-JME-16-004, CERN, 2016.

[43] J. Alwall et al., "The automated computation of tree-level and next-to-leading order differential cross sections, and their matching to parton shower simulations", *JHEP* **07** (2014) 079, doi:10.1007/JHEP07(2014)079, arXiv:1405.0301.

[44] J. Alwall et al., "Comparative study of various algorithms for the merging of parton showers and matrix elements in hadronic collisions", *Eur. Phys. J. C* **53** (2008) 473, doi:10.1140/epjc/s10052-007-0490-5, arXiv:0706.2569.

[45] R. Frederix and S. Frixione, "Merging meets matching in MC@NLO", *JHEP* **12** (2012) 061, doi:10.1007/JHEP12(2012)061, arXiv:1209.6215.

[46] P. Nason, "A new method for combining NLO QCD with shower Monte Carlo algorithms", *JHEP* **11** (2004) 040, doi:10.1088/1126-6708/2004/11/040, arXiv:hep-ph/0409146.

[47] S. Frixione, P. Nason, and C. Oleari, "Matching NLO QCD computations with Parton Shower simulations: the POWHEG method", *JHEP* **11** (2007) 070, doi:10.1088/1126-6708/2007/11/070, arXiv:0709.2092.

[48] S. Alioli, P. Nason, C. Oleari, and E. Re, "A general framework for implementing NLO calculations in shower Monte Carlo programs: the POWHEG BOX", *JHEP* **06** (2010) 043, doi:10.1007/JHEP06(2010)043, arXiv:1002.2581.

[49] S. Alioli, P. Nason, C. Oleari, and E. Re, "NLO single-top production matched with shower in POWHEG: s- and t-channel contributions", *JHEP* **09** (2009) 111, doi:10.1088/1126-6708/2009/09/111, arXiv:0907.4076. [Erratum: doi:10.1007/JHEP02(2010)011].

[50] E. Re, "Single-top Wt-channel production matched with parton showers using the POWHEG method", *Eur. Phys. J. C* **71** (2011) 1547, doi:10.1140/epjc/s10052-011-1547-z, arXiv:1009.2450.

[51] GEANT4 Collaboration, "GEANT4 — a simulation toolkit", *Nucl. Instrum. Meth. A* **506** (2003) 250, doi:10.1016/S0168-9002(03)01368-8.

[52] T. Melia, P. Nason, R. Rontsch, and G. Zanderighi, "W^+W^-, WZ and ZZ production in the POWHEG BOX", *JHEP* **11** (2011) 078, doi:10.1007/JHEP11(2011)078, arXiv:1107.5051.

[53] M. Beneke, P. Falgari, S. Klein, and C. Schwinn, "Hadronic top-quark pair production with NNLL threshold resummation", *Nucl. Phys. B* **855** (2012) 695, doi:10.1016/j.nuclphysb.2011.10.021, arXiv:1109.1536.

[54] M. Cacciari et al., "Top-pair production at hadron colliders with next-to-next-to-leading logarithmic soft-gluon resummation", *Phys. Lett. B* **710** (2012) 612, doi:10.1016/j.physletb.2012.03.013, arXiv:1111.5869.

[55] P. Bärnreuther, M. Czakon, and A. Mitov, "Percent Level Precision Physics at the Tevatron: First Genuine NNLO QCD Corrections to $q\bar{q} \to t\bar{t} + X$", *Phys. Rev. Lett.* **109** (2012) 132001, doi:10.1103/PhysRevLett.109.132001, arXiv:1204.5201.

[56] M. Czakon and A. Mitov, "NNLO corrections to top-pair production at hadron colliders: the all-fermionic scattering channels", *JHEP* **12** (2012) 054, doi:10.1007/JHEP12(2012)054, arXiv:1207.0236.

[57] M. Czakon and A. Mitov, "NNLO corrections to top pair production at hadron colliders: the quark-gluon reaction", *JHEP* **01** (2013) 080, doi:10.1007/JHEP01(2013)080, arXiv:1210.6832.

[58] M. Czakon, P. Fiedler, and A. Mitov, "Total Top-Quark Pair-Production Cross Section at Hadron Colliders Through $O(\alpha_S^4)$", *Phys. Rev. Lett.* **110** (2013) 252004, doi:10.1103/PhysRevLett.110.252004, arXiv:1303.6254.

[59] R. Gavin, Y. Li, F. Petriello, and S. Quackenbush, "W Physics at the LHC with FEWZ 2.1", *Comput. Phys. Commun.* **184** (2013) 208, doi:10.1016/j.cpc.2012.09.005, arXiv:1201.5896.

[60] R. Gavin, Y. Li, F. Petriello, and S. Quackenbush, "FEWZ 2.0: A code for hadronic Z production at next-to-next-to-leading order", *Comput. Phys. Commun.* **182** (2011) 2388, doi:10.1016/j.cpc.2011.06.008, arXiv:1011.3540.

[61] W. Beenakker, R. Höpker, M. Spira, and P. M. Zerwas, "Squark and gluino production at hadron colliders", *Nucl. Phys. B* **492** (1997) 51, doi:10.1016/S0550-3213(97)00084-9, arXiv:hep-ph/9610490.

[62] A. Kulesza and L. Motyka, "Threshold resummation for squark-antisquark and gluino-pair production at the LHC", *Phys. Rev. Lett.* **102** (2009) 111802, doi:10.1103/PhysRevLett.102.111802, arXiv:0807.2405.

[63] A. Kulesza and L. Motyka, "Soft gluon resummation for the production of gluino-gluino and squark-antisquark pairs at the LHC", *Phys. Rev. D* **80** (2009) 095004, doi:10.1103/PhysRevD.80.095004, arXiv:0905.4749.

[64] W. Beenakker et al., "Soft-gluon resummation for squark and gluino hadroproduction", *JHEP* **12** (2009) 041, doi:10.1088/1126-6708/2009/12/041, arXiv:0909.4418.

[65] W. Beenakker et al., "Squark and gluino hadroproduction", *Int. J. Mod. Phys. A* **26** (2011) 2637, doi:10.1142/S0217751X11053560, arXiv:1105.1110.

[66] T. Sjöstrand et al., "An Introduction to PYTHIA 8.2", *Comput. Phys. Commun.* **191** (2015) 159, doi:10.1016/j.cpc.2015.01.024, arXiv:1410.3012.

[67] CMS Collaboration, "Fast simulation of the CMS detector", *J. Phys. Conf. Ser.* **219** (2010) 032053, doi:10.1088/1742-6596/219/3/032053.

[68] CMS Collaboration, "Comparison of the fast simulation of CMS with the first LHC data", CMS Detector Performance Summary CMS-DP-2010-039, CERN, 2010.

[69] NNPDF Collaboration, "Parton distributions for the LHC Run II", *JHEP* **04** (2015) 040, doi:10.1007/JHEP04(2015)040, arXiv:1410.8849.

[70] S. Catani, D. de Florian, M. Grazzini, and P. Nason, "Soft gluon resummation for Higgs boson production at hadron colliders", *JHEP* **07** (2003) 028, doi:10.1088/1126-6708/2003/07/028, arXiv:hep-ph/0306211.

[71] M. Cacciari et al., "The $\mathrm{t\bar{t}}$ cross-section at 1.8 TeV and 1.96 TeV: a study of the systematics due to parton densities and scale dependence", *JHEP* **04** (2004) 068, doi:10.1088/1126-6708/2004/04/068, arXiv:hep-ph/0303085.

[72] CMS Collaboration, "CMS Luminosity Measurements for the 2016 Data Taking Period", CMS Physics Analysis Summary CMS-PAS-LUM-17-001, CERN, 2017.

[73] CMS Collaboration, "Search for new physics in the multijet and missing transverse momentum final state in proton-proton collisions at $\sqrt{s} = 7$ TeV", *Phys. Rev. Lett.* **109** (2012) 171803, doi:10.1103/PhysRevLett.109.171803, arXiv:1207.1898.

[74] Particle Data Group, C. Patrignani et al., "Review of particle physics", *Chin. Phys. C* **40** (2016) 100001, doi:10.1088/1674-1137/40/10/100001.

[75] CMS Collaboration, " Observation of top quark pairs produced in association with a vector boson in pp collisions at $\sqrt{s} = 8$ TeV", *JHEP* **01** (2016) 096, doi:10.1007/JHEP01(2016)096, arXiv:1510.01131.

[76] CMS Collaboration, "Search for gluino mediated bottom- and top-squark production in multijet final states in pp collisions at 8 TeV", *Phys. Lett. B* **725** (2013) 243, doi:10.1016/j.physletb.2013.06.058, arXiv:1305.2390.

[77] G. Cowan, K. Cranmer, E. Gross, and O. Vitells, "Asymptotic formulae for likelihood-based tests of new physics", *Eur. Phys. J. C* **71** (2011) 1554, doi:10.1140/epjc/s10052-011-1554-0, arXiv:1007.1727. [Erratum: doi:10.1140/epjc/s10052-013-2501-z].

[78] T. Junk, "Confidence level computation for combining searches with small statistics", *Nucl. Instrum. Meth. A* **434** (1999) 435, doi:10.1016/S0168-9002(99)00498-2, arXiv:hep-ex/9902006.

[79] A. L. Read, "Presentation of search results: the CL_s technique", *J. Phys. G* **28** (2002) 2693, doi:10.1088/0954-3899/28/10/313.

[80] C. Borschensky et al., "Squark and gluino production cross sections in pp collisions at $\sqrt{s}$ = 13, 14, 33 and 100 TeV", *Eur. Phys. J. C* **74** (2014) 3174, doi:10.1140/epjc/s10052-014-3174-y, arXiv:1407.5066.

A Selection efficiency for representative signal models

Tables A.1 and A.2 present cumulative selection efficiencies for representative simplified models of gluino and squark pair production, respectively.

Table A.1: Absolute cumulative efficiencies in % for each step of the event selection process for representative models of gluino pair production. The uncertainties are statistical. Uncertainties reported as 0.0 correspond to values less than 0.05%.

Selection	$pp \to \tilde{g}\tilde{g}, \tilde{g} \to t\bar{t}\tilde{\chi}_1^0$ $m_{\tilde{g}} = 1500\,\text{GeV}$ $m_{\tilde{\chi}_1^0} = 100\,\text{GeV}$	$pp \to \tilde{g}\tilde{g}, \tilde{g} \to b\bar{b}\tilde{\chi}_1^0$ $m_{\tilde{g}} = 1500\,\text{GeV}$ $m_{\tilde{\chi}_1^0} = 100\,\text{GeV}$	$pp \to \tilde{g}\tilde{g}, \tilde{g} \to q\bar{q}\tilde{\chi}_1^0$ $m_{\tilde{g}} = 1400\,\text{GeV}$ $m_{\tilde{\chi}_1^0} = 100\,\text{GeV}$
$N_{\text{jet}} \geq 2$	100.0 ± 0.0	100.0 ± 0.0	100.00 ± 0.0
$H_{\text{T}} > 300\,\text{GeV}$	100.0 ± 0.0	100.0 ± 0.0	100.0 ± 0.0
$H_{\text{T}}^{\text{miss}} > 300\,\text{GeV}$	76.7 ± 0.3	80.3 ± 0.4	80.0 ± 0.3
$N_{\text{muon}} = 0$	48.6 ± 0.4	79.8 ± 0.4	80.0 ± 0.3
$N_{\text{isolated tracks}}^{(\text{muon})} = 0$	47.8 ± 0.4	79.6 ± 0.4	79.9 ± 0.3
$N_{\text{electron}} = 0$	30.7 ± 0.3	79.2 ± 0.4	79.5 ± 0.3
$N_{\text{isolated tracks}}^{(\text{electron})} = 0$	29.7 ± 0.3	78.7 ± 0.4	79.1 ± 0.3
$N_{\text{isolated tracks}}^{(\text{hadron})} = 0$	28.3 ± 0.3	78.0 ± 0.4	78.3 ± 0.3
$\Delta\phi_{H_{\text{T}}^{\text{miss}},j_1} > 0.5$	27.7 ± 0.3	76.7 ± 0.4	76.9 ± 0.3
$\Delta\phi_{H_{\text{T}}^{\text{miss}},j_2} > 0.5$	25.2 ± 0.3	69.2 ± 0.5	69.8 ± 0.3
$\Delta\phi_{H_{\text{T}}^{\text{miss}},j_3} > 0.3$	23.7 ± 0.3	63.9 ± 0.5	64.4 ± 0.3
$\Delta\phi_{H_{\text{T}}^{\text{miss}},j_4} > 0.3$	22.1 ± 0.3	58.6 ± 0.5	59.4 ± 0.3
Event quality filter	21.8 ± 0.3	57.7 ± 0.5	58.7 ± 0.3
Selection	$pp \to \tilde{g}\tilde{g}, \tilde{g} \to t\bar{t}\tilde{\chi}_1^0$ $m_{\tilde{g}} = 1200\,\text{GeV}$ $m_{\tilde{\chi}_1^0} = 800\,\text{GeV}$	$pp \to \tilde{g}\tilde{g}, \tilde{g} \to b\bar{b}\tilde{\chi}_1^0$ $m_{\tilde{g}} = 1000\,\text{GeV}$ $m_{\tilde{\chi}_1^0} = 900\,\text{GeV}$	$pp \to \tilde{g}\tilde{g}, \tilde{g} \to q\bar{q}\tilde{\chi}_1^0$ $m_{\tilde{g}} = 1000\,\text{GeV}$ $m_{\tilde{\chi}_1^0} = 800\,\text{GeV}$
$N_{\text{jet}} \geq 2$	100.0 ± 0.0	92.5 ± 0.1	99.6 ± 0.0
$H_{\text{T}} > 300\,\text{GeV}$	99.0 ± 0.0	38.6 ± 0.1	81.3 ± 0.1
$H_{\text{T}}^{\text{miss}} > 300\,\text{GeV}$	14.9 ± 0.1	$14.1 \pm$ 01	19.1 ± 0.1
$N_{\text{muon}} = 0$	9.6 ± 0.1	13.9 ± 0.1	19.1 ± 0.1
$N_{\text{isolated tracks}}^{(\text{muon})} = 0$	9.2 ± 0.1	13.6 ± 0.1	19.1 ± 0.1
$N_{\text{electron}} = 0$	6.2 ± 0.1	13.4 ± 0.1	19.0 ± 0.1
$N_{\text{isolated tracks}}^{(\text{electron})} = 0$	5.8 ± 0.1	13.1 ± 0.1	18.8 ± 0.1
$N_{\text{isolated tracks}}^{(\text{hadron})} = 0$	5.3 ± 0.1	12.8 ± 0.1	18.4 ± 0.1
$\Delta\phi_{H_{\text{T}}^{\text{miss}},j_1} > 0.5$	5.3 ± 0.1	12.8 ± 0.1	18.4 ± 0.1
$\Delta\phi_{H_{\text{T}}^{\text{miss}},j_2} > 0.5$	4.5 ± 0.1	11.4 ± 0.1	16.9 ± 0.1
$\Delta\phi_{H_{\text{T}}^{\text{miss}},j_3} > 0.3$	4.0 ± 0.1	10.4 ± 0.1	15.8 ± 0.1
$\Delta\phi_{H_{\text{T}}^{\text{miss}},j_4} > 0.3$	3.6 ± 0.1	9.6 ± 0.1	14.8 ± 0.1
Event quality filter	3.5 ± 0.1	9.4 ± 0.1	14.6 ± 0.1

Table A.2: Absolute cumulative efficiencies in % for each step of the event selection process for representative models of squark pair production. The uncertainties are statistical. Uncertainties reported as 0.0 correspond to values less than 0.05%.

Selection	$pp \to \tilde{t}\bar{\tilde{t}}, \tilde{t} \to t\tilde{\chi}_1^0$ $m_{\tilde{t}} = 700\,\text{GeV}$ $m_{\tilde{\chi}_1^0} = 50\,\text{GeV}$	$pp \to \tilde{b}\bar{\tilde{b}}, \tilde{b} \to b\tilde{\chi}_1^0$ $m_{\tilde{b}} = 650\,\text{GeV}$ $m_{\tilde{\chi}_1^0} = 1\,\text{GeV}$	$pp \to \tilde{q}\bar{\tilde{q}}, \tilde{q} \to q\tilde{\chi}_1^0$ $m_{\tilde{q}} = 1000\,\text{GeV}$ $m_{\tilde{\chi}_1^0} = 100\,\text{GeV}$
$N_{\text{jet}} \geq 2$	99.8 ± 0.0	98.2 ± 0.1	98.9 ± 0.1
$H_{\text{T}} > 300\,\text{GeV}$	96.4 ± 0.1	95.4 ± 0.1	98.6 ± 0.1
$H_{\text{T}}^{\text{miss}} > 300\,\text{GeV}$	57.8 ± 0.3	59.8 ± 0.2	80.0 ± 0.3
$N_{\text{muon}} = 0$	46.6 ± 0.3	59.6 ± 0.2	79.9 ± 0.3
$N_{\text{isolated tracks}}^{(\text{muon})} = 0$	46.1 ± 0.3	59.5 ± 0.2	79.8 ± 0.3
$N_{\text{electron}} = 0$	37.4 ± 0.3	59.2 ± 0.2	79.6 ± 0.3
$N_{\text{isolated tracks}}^{(\text{electron})} = 0$	36.9 ± 0.3	59.0 ± 0.2	79.3 ± 0.3
$N_{\text{isolated tracks}}^{(\text{hadron})} = 0$	35.8 ± 0.3	58.5 ± 0.2	78.7 ± 0.3
$\Delta\phi_{H_{\text{T}}^{\text{miss}},j_1} > 0.5$	35.7 ± 0.3	58.4 ± 0.2	78.6 ± 0.3
$\Delta\phi_{H_{\text{T}}^{\text{miss}},j_2} > 0.5$	34.0 ± 0.3	55.7 ± 0.2	74.5 ± 0.3
$\Delta\phi_{H_{\text{T}}^{\text{miss}},j_3} > 0.3$	33.1 ± 0.3	53.3 ± 0.2	70.6 ± 0.3
$\Delta\phi_{H_{\text{T}}^{\text{miss}},j_4} > 0.3$	31.8 ± 0.3	51.6 ± 0.2	67.9 ± 0.3
Event quality filter	31.4 ± 0.3	50.8 ± 0.3	67.1 ± 0.3
Selection	$pp \to \tilde{t}\bar{\tilde{t}}, \tilde{t} \to t\tilde{\chi}_1^0$ $m_{\tilde{t}} = 300\,\text{GeV}$ $m_{\tilde{\chi}_1^0} = 200\,\text{GeV}$	$pp \to \tilde{b}\bar{\tilde{b}}, \tilde{b} \to b\tilde{\chi}_1^0$ $m_{\tilde{b}} = 500\,\text{GeV}$ $m_{\tilde{\chi}_1^0} = 300\,\text{GeV}$	$pp \to \tilde{q}\bar{\tilde{q}}, \tilde{q} \to q\tilde{\chi}_1^0$ $m_{\tilde{q}} = 700\,\text{GeV}$ $m_{\tilde{\chi}_1^0} = 400\,\text{GeV}$
$N_{\text{jet}} \geq 2$	86.9 ± 0.0	96.0 ± 0.1	98.0 ± 0.0
$H_{\text{T}} > 300\,\text{GeV}$	23.3 ± 0.0	68.0 ± 0.1	91.3 ± 0.1
$H_{\text{T}}^{\text{miss}} > 300\,\text{GeV}$	2.84 ± 0.0	15.6 ± 0.1	43.8 ± 0.1
$N_{\text{muon}} = 0$	2.16 ± 0.0	15.6 ± 0.1	43.8 ± 0.1
$N_{\text{isolated tracks}}^{(\text{muon})} = 0$	2.10 ± 0.0	15.5 ± 0.1	43.7 ± 0.1
$N_{\text{electron}} = 0$	1.60 ± 0.0	15.4 ± 0.1	43.5 ± 0.1
$N_{\text{isolated tracks}}^{(\text{electron})} = 0$	1.52 ± 0.0	15.3 ± 0.1	43.4 ± 0.1
$N_{\text{isolated tracks}}^{(\text{hadron})} = 0$	1.41 ± 0.0	15.2 ± 0.1	43.0 ± 0.1
$\Delta\phi_{H_{\text{T}}^{\text{miss}},j_1} > 0.5$	1.40 ± 0.0	15.1 ± 0.1	42.9 ± 0.1
$\Delta\phi_{H_{\text{T}}^{\text{miss}},j_2} > 0.5$	1.03 ± 0.0	14.1 ± 0.1	41.1 ± 0.1
$\Delta\phi_{H_{\text{T}}^{\text{miss}},j_3} > 0.3$	0.85 ± 0.0	13.5 ± 0.1	39.6 ± 0.1
$\Delta\phi_{H_{\text{T}}^{\text{miss}},j_4} > 0.3$	0.73 ± 0.0	13.1 ± 0.1	38.4 ± 0.1
Event quality filter	0.72 ± 0.0	12.9 ± 0.1	37.9 ± 0.1

B Prefit background predictions

Tables B.1–B.5 present the predictions for the number of standard model background events in each of the 174 search bins of the analysis, along with the observed numbers of events. The corresponding information for the 12 aggregate search regions is presented in Table B.6.

Table B.1: Observed number of events and pre-fit background predictions in the $N_{\text{jet}} = 2$ search bins.

Bin	$H_{\text{T}}^{\text{miss}}$ [GeV]	H_{T} [GeV]	N_{jet}	$N_{\text{b-jet}}$	Lost-e/μ	$\tau \to$ had	$Z \to \nu\bar{\nu}$	QCD	Total Pred.	Obs.
1	300-350	300-500	2	0	$4069^{+67+320}_{-67-320}$	$2744^{+37+510}_{-37-500}$	$13231^{+67+760}_{-66-740}$	$326^{+12+170}_{-12-120}$	$20370^{+120+980}_{-120-960}$	21626
2	300-350	500-1000	2	0	326^{+22+36}_{-22-36}	226^{+11+43}_{-11-42}	944^{+18+55}_{-18-54}	45^{+2+24}_{-2-17}	1541^{+37+82}_{-37-79}	1583
3	300-350	1000+	2	0	$15.2^{+5.8+2.3}_{-5.1-2.3}$	$8.7^{+2.1+2.1}_{-2.0-2.1}$	$50.9^{+4.5+4.4}_{-4.1-3.8}$	$1.57^{+0.16+0.84}_{-0.16-0.61}$	$76.3^{+9.1+5.5}_{-8.2-5.0}$	102
4	350-500	350-500	2	0	$2049^{+46+160}_{-46-160}$	$1553^{+27+290}_{-27-290}$	$9347^{+57+540}_{-57-520}$	126^{+4+67}_{-4-48}	$13076^{+93+630}_{-93-620}$	14019
5	350-500	500-1000	2	0	631^{+25+54}_{-25-54}	439^{+14+84}_{-14-84}	$2502^{+30+150}_{-30-140}$	43^{+7+22}_{-7-16}	$3615^{+49+180}_{-49-170}$	3730
6	350-500	1000+	2	0	$13.5^{+4.9+1.9}_{-4.3-1.9}$	$13.4^{+2.4+2.6}_{-2.3-2.6}$	$94.0^{+6.2+7.9}_{-5.8-6.9}$	$1.30^{+0.06+0.68}_{-0.06-0.49}$	$122.1^{+9.5+8.6}_{-8.8-7.6}$	139
7	500-750	500-1000	2	0	303^{+17+29}_{-17-29}	247^{+10+48}_{-10-47}	$2328^{+30+170}_{-29-160}$	$4.5^{+0.1+2.4}_{-0.1-1.7}$	$2883^{+40+180}_{-40-170}$	3018
8	500-750	1000+	2	0	$5.8^{+2.7+1.5}_{-2.2-1.5}$	$5.3^{+1.4+1.3}_{-1.3-1.3}$	$66.2^{+5.4+5.3}_{-5.0-5.1}$	$0.03^{+0.02+0.02}_{-0.02-0.01}$	$77.3^{+6.8+5.7}_{-6.1-5.4}$	96
9	750+	750-1500	2	0	$17.3^{+4.5+3.0}_{-4.1-3.0}$	$17.4^{+2.5+4.5}_{-2.4-4.5}$	295^{+11+41}_{-11-38}	$0.35^{+0.06+0.18}_{-0.06-0.13}$	330^{+13+42}_{-12-38}	272
10	750+	1500+	2	0	$0.0^{+1.8+0.0}_{-0.0-0.0}$	$0.38^{+0.54+0.09}_{-0.29-0.09}$	$12.6^{+3.0+2.1}_{-2.4-1.9}$	$0.01^{+0.01+0.00}_{-0.01-0.00}$	$13.0^{+3.8+2.1}_{-2.5-1.9}$	12
11	300-350	300-500	2	1	370^{+21+31}_{-21-31}	288^{+11+63}_{-11-63}	1361^{+7+140}_{-7-140}	44^{+6+25}_{-6-17}	$2063^{+33+160}_{-33-160}$	1904
12	300-350	500-1000	2	1	51^{+10+7}_{-10-7}	$31.6^{+4.2+7.2}_{-4.2-7.2}$	97^{+2+10}_{-2-10}	$6.7^{+2.7+3.7}_{-2.7-2.5}$	186^{+15+15}_{-14-14}	186
13	300-350	1000+	2	1	$1.1^{+2.3+0.2}_{-1.1-0.0}$	$2.0^{+1.1+0.5}_{-1.0-0.5}$	$5.23^{+0.46+0.63}_{-0.42-0.59}$	$0.33^{+0.02+0.18}_{-0.02-0.13}$	$8.7^{+3.4+0.9}_{-2.1-0.8}$	13
14	350-500	350-500	2	1	215^{+16+19}_{-16-19}	179^{+9+39}_{-9-39}	962^{+6+99}_{-6-98}	20^{+2+11}_{-2-8}	$1376^{+26+110}_{-26-110}$	1212
15	350-500	500-1000	2	1	$69.8^{+9.9+7.5}_{-9.8-7.5}$	$43.3^{+4.4+9.7}_{-4.4-9.6}$	257^{+3+27}_{-3-26}	$8.5^{+3.0+4.8}_{-3.0-3.2}$	379^{+15+30}_{-15-29}	409
16	350-500	1000+	2	1	$3.7^{+2.5+0.7}_{-1.9-0.7}$	$3.1^{+1.1+0.9}_{-1.0-0.9}$	$9.7^{+0.6+1.2}_{-0.6-1.1}$	$0.13^{+0.04+0.07}_{-0.04-0.05}$	$16.6^{+3.7+1.6}_{-3.0-1.6}$	27
17	500-750	500-1000	2	1	$28.9^{+5.8+3.3}_{-5.6-3.3}$	$26.0^{+2.9+5.8}_{-2.9-5.8}$	240^{+3+27}_{-3-26}	$1.48^{+0.18+0.83}_{-0.18-0.56}$	296^{+9+28}_{-9-27}	321
18	500-750	1000+	2	1	$5.1^{+6.2+1.6}_{-4.1-1.6}$	$0.36^{+0.55+0.12}_{-0.30-0.12}$	$6.81^{+0.56+0.80}_{-0.52-0.78}$	$0.03^{+0.03+0.02}_{-0.03-0.00}$	$12.3^{+6.8+1.8}_{-4.5-1.7}$	14
19	750+	750-1500	2	1	$3.8^{+2.2+0.8}_{-1.7-0.8}$	$4.1^{+1.5+1.1}_{-1.4-1.1}$	$30.4^{+1.1+5.0}_{-1.1-4.7}$	$0.10^{+0.03+0.06}_{-0.03-0.04}$	$38.4^{+3.9+5.1}_{-3.3-4.8}$	31
20	750+	1500+	2	1	$0.0^{+1.4+0.0}_{-0.0-0.0}$	$0.34^{+0.51+0.13}_{-0.22-0.13}$	$1.29^{+0.31+0.24}_{-0.25-0.23}$	$0.00^{+0.01+0.00}_{-0.00-0.00}$	$1.6^{+2.0+0.3}_{-0.3-0.3}$	1
21	300-350	300-500	2	2	$14.1^{+4.5+2.6}_{-4.0-2.6}$	$12.9^{+2.3+2.8}_{-2.2-2.8}$	49^{+0+17}_{-0-17}	$3.0^{+0.8+3.6}_{-0.8-2.1}$	79^{+7+18}_{-6-18}	122
22	300-350	500-1000	2	2	$2.8^{+2.4+0.9}_{-1.7-0.9}$	$2.0^{+1.1+1.0}_{-0.9-1.0}$	$3.5^{+0.1+1.2}_{-0.1-1.2}$	$0.57^{+0.17+0.69}_{-0.17-0.40}$	$8.9^{+3.5+2.0}_{-2.6-1.9}$	11
23	300-350	1000+	2	2	$0.0^{+2.2+0.0}_{-0.0-0.0}$	$0.00^{+0.46+0.00}_{-0.00-0.00}$	$0.19^{+0.02+0.07}_{-0.01-0.07}$	$0.03^{+0.01+0.04}_{-0.01-0.02}$	$0.2^{+2.6+0.1}_{-0.0-0.1}$	0
24	350-500	350-500	2	2	$11.4^{+4.5+2.5}_{-3.9-2.5}$	$6.3^{+1.7+2.1}_{-1.6-2.1}$	35^{+0+12}_{-0-12}	$1.0^{+0.5+1.2}_{-0.5-0.6}$	53^{+6+13}_{-6-13}	84
25	350-500	500-1000	2	2	$6.1^{+2.9+1.5}_{-2.4-1.5}$	$2.9^{+1.2+0.8}_{-1.1-0.8}$	$9.3^{+0.1+3.3}_{-0.1-3.3}$	$0.44^{+0.05+0.52}_{-0.05-0.39}$	$18.7^{+4.1+3.8}_{-3.5-3.7}$	23
26	350-500	1000+	2	2	$0.0^{+1.1+0.0}_{-0.0-0.0}$	$0.00^{+0.46+0.00}_{-0.00-0.00}$	$0.35^{+0.02+0.13}_{-0.02-0.13}$	$0.06^{+0.04+0.08}_{-0.04-0.02}$	$0.4^{+1.5+0.1}_{-0.0-0.1}$	2
27	500-750	500-1000	2	2	$1.4^{+2.9+0.4}_{-1.4-0.0}$	$2.03^{+0.84+0.61}_{-0.70-0.61}$	$8.6^{+0.1+3.1}_{-0.1-3.1}$	$0.03^{+0.01+0.04}_{-0.01-0.03}$	$12.1^{+3.7+3.2}_{-2.1-3.2}$	16
28	500-750	1000+	2	2	$0.0^{+2.2+0.0}_{-0.0-0.0}$	$0.00^{+0.46+0.00}_{-0.00-0.00}$	$0.24^{+0.02+0.09}_{-0.02-0.09}$	$0.00^{+0.01+0.00}_{-0.00-0.00}$	$0.2^{+2.7+0.1}_{-0.0-0.1}$	0
29	750+	750-1500	2	2	$0.0^{+1.6+0.0}_{-0.0-0.0}$	$0.07^{+0.46+0.07}_{-0.04-0.06}$	$1.09^{+0.04+0.41}_{-0.04-0.41}$	$0.01^{+0.01+0.01}_{-0.01-0.00}$	$1.2^{+2.1+0.4}_{-0.1-0.4}$	4
30	750+	1500+	2	2	$0.0^{+2.0+0.0}_{-0.0-0.0}$	$0.00^{+0.46+0.00}_{-0.00-0.00}$	$0.05^{+0.01+0.02}_{-0.01-0.02}$	$0.00^{+0.01+0.00}_{-0.00-0.00}$	$0.0^{+2.5+0.0}_{-0.0-0.0}$	0

Table B.2: Observed number of events and pre-fit background predictions in the $3 \leq N_{\text{jet}} \leq 4$ search bins.

Bin	$H_{\text{T}}^{\text{miss}}$ [GeV]	H_{T} [GeV]	N_{jet}	$N_{\text{b-jet}}$	Lost-e/μ	$\tau \to$ had	$Z \to \nu\bar{\nu}$	QCD	Total Pred.	Obs.
31	300-350	300-500	3-4	0	$2830^{+45+200}_{-45-200}$	$2152^{+29+160}_{-29-150}$	$8353^{+52+480}_{-52-470}$	$273^{+68+120}_{-68-100}$	$13608^{+110+560}_{-110-540}$	14520
32	300-350	500-1000	3-4	0	$1125^{+25+120}_{-25-120}$	$909^{+18+100}_{-18-100}$	$2487^{+29+140}_{-28-140}$	119^{+8+51}_{-8-45}	$4640^{+52+220}_{-52-210}$	4799
33	300-350	1000+	3-4	0	$72.7^{+7.1+6.1}_{-7.1-6.1}$	$65.3^{+5.2+6.4}_{-5.2-6.3}$	176^{+8+14}_{-8-12}	41^{+2+18}_{-2-16}	356^{+15+24}_{-15-22}	354
34	350-500	350-500	3-4	0	$1439^{+37+110}_{-37-110}$	$930^{+19+120}_{-19-110}$	$5014^{+41+280}_{-41-280}$	114^{+6+48}_{-6-43}	$7496^{+70+330}_{-69-320}$	7973
35	350-500	500-1000	3-4	0	$1402^{+27+140}_{-27-140}$	$1253^{+22+120}_{-22-120}$	$4811^{+40+270}_{-40-260}$	80^{+9+34}_{-9-31}	$7547^{+65+330}_{-64-320}$	7735
36	350-500	1000+	3-4	0	103^{+8+11}_{-8-11}	$77.0^{+5.9+7.6}_{-5.9-7.5}$	303^{+11+24}_{-10-21}	24^{+1+10}_{-1-9}	506^{+18+30}_{-17-26}	490
37	500-750	500-1000	3-4	0	339^{+15+33}_{-15-33}	297^{+10+26}_{-10-26}	$2143^{+28+150}_{-28-140}$	$5.5^{+0.2+2.3}_{-0.2-2.1}$	$2785^{+37+160}_{-37-150}$	2938
38	500-750	1000+	3-4	0	$33.8^{+4.4+3.6}_{-4.3-3.6}$	$30.5^{+3.4+2.9}_{-3.4-2.9}$	219^{+10+16}_{-9-15}	$1.29^{+0.53+0.55}_{-0.53-0.49}$	284^{+12+17}_{-12-16}	303
39	750+	750-1500	3-4	0	$28.2^{+4.4+3.7}_{-4.3-3.7}$	$26.0^{+2.9+3.4}_{-2.9-3.4}$	319^{+11+44}_{-11-40}	$0.32^{+0.03+0.14}_{-0.03-0.12}$	373^{+14+44}_{-13-41}	334
40	750+	1500+	3-4	0	$2.9^{+2.0+0.7}_{-1.5-0.7}$	$1.38^{+0.66+0.17}_{-0.48-0.17}$	$27.8^{+3.9+4.1}_{-3.5-3.8}$	$0.10^{+0.01+0.04}_{-0.01-0.04}$	$32.2^{+4.8+4.2}_{-4.0-3.9}$	46
41	300-350	300-500	3-4	1	746^{+25+55}_{-25-55}	627^{+15+48}_{-15-47}	1235^{+8+130}_{-8-120}	59^{+4+24}_{-4-22}	$2667^{+41+150}_{-41-150}$	2677
42	300-350	500-1000	3-4	1	296^{+15+25}_{-15-25}	262^{+9+27}_{-9-27}	385^{+4+39}_{-4-39}	38^{+4+15}_{-4-14}	981^{+24+56}_{-24-56}	1048
43	300-350	1000+	3-4	1	$20.8^{+4.1+2.1}_{-4.0-2.1}$	$19.0^{+2.6+1.8}_{-2.5-1.8}$	$27.6^{+1.3+3.2}_{-1.2-3.0}$	$11.4^{+0.8+4.7}_{-0.8-4.4}$	$78.8^{+6.9+6.3}_{-6.6-6.0}$	92
44	350-500	350-500	3-4	1	321^{+17+25}_{-17-25}	263^{+10+22}_{-10-21}	738^{+6+74}_{-6-74}	$22.3^{+1.4+9.1}_{-1.4-8.5}$	1343^{+28+82}_{-28-81}	1332
45	350-500	500-1000	3-4	1	329^{+14+26}_{-14-26}	324^{+11+26}_{-11-26}	737^{+6+74}_{-6-74}	$17.6^{+3.4+7.2}_{-3.4-6.7}$	1407^{+26+83}_{-26-83}	1515
46	350-500	1000+	3-4	1	$20.4^{+4.0+2.0}_{-3.8-2.0}$	$19.9^{+2.9+1.8}_{-2.9-1.7}$	$47.5^{+1.7+5.5}_{-1.6-5.1}$	$5.7^{+0.5+2.3}_{-0.5-2.2}$	$93.4^{+7.1+6.5}_{-6.9-6.2}$	113
47	500-750	500-1000	3-4	1	$69.7^{+7.4+6.6}_{-7.3-6.6}$	$56.0^{+4.1+5.0}_{-4.1-4.9}$	322^{+4+35}_{-4-35}	$1.34^{+0.10+0.55}_{-0.10-0.51}$	449^{+12+36}_{-12-36}	472
48	500-750	1000+	3-4	1	$15.3^{+3.4+1.9}_{-3.3-1.9}$	$7.0^{+1.4+0.7}_{-1.4-0.7}$	$34.4^{+1.5+3.8}_{-1.4-3.8}$	$0.38^{+0.14+0.16}_{-0.14-0.15}$	$57.0^{+5.1+4.4}_{-4.9-4.3}$	57
49	750+	750-1500	3-4	1	$3.3^{+1.5+0.5}_{-1.3-0.5}$	$4.8^{+1.3+0.8}_{-1.2-0.8}$	$48.5^{+1.7+7.9}_{-1.7-7.3}$	$0.13^{+0.01+0.05}_{-0.01-0.05}$	$56.8^{+3.3+7.9}_{-3.0-7.4}$	61
50	750+	1500+	3-4	1	$1.0^{+1.2+0.3}_{-0.7-0.3}$	$0.77^{+0.75+0.16}_{-0.59-0.16}$	$4.40^{+0.62+0.75}_{-0.55-0.71}$	$0.03^{+0.01+0.01}_{-0.01-0.01}$	$6.2^{+2.0+0.8}_{-1.4-0.8}$	8
51	300-350	300-500	3-4	2	137^{+11+11}_{-11-11}	133^{+7+11}_{-7-11}	145^{+1+26}_{-1-26}	$9.0^{+1.1+3.9}_{-1.1-3.4}$	424^{+18+31}_{-17-31}	464
52	300-350	500-1000	3-4	2	$92.3^{+9.1+9.5}_{-9.0-9.5}$	$85.6^{+5.7+7.5}_{-5.7-7.4}$	$53.0^{+0.6+9.6}_{-0.6-9.6}$	$3.8^{+1.2+1.6}_{-1.2-1.4}$	235^{+15+16}_{-15-15}	227
53	300-350	1000+	3-4	2	$3.4^{+2.2+0.8}_{-1.7-0.8}$	$2.41^{+0.91+0.50}_{-0.78-0.50}$	$3.95^{+0.18+0.75}_{-0.17-0.73}$	$2.23^{+0.18+0.96}_{-0.18-0.86}$	$12.0^{+3.1+1.6}_{-2.5-1.5}$	17
54	350-500	350-500	3-4	2	$39.6^{+6.1+3.8}_{-5.9-3.8}$	$39.8^{+3.9+3.8}_{-3.8-3.8}$	84^{+1+15}_{-1-15}	$2.7^{+0.6+1.1}_{-0.6-1.0}$	166^{+10+16}_{-10-16}	208
55	350-500	500-1000	3-4	2	$83.9^{+8.2+7.8}_{-8.1-7.8}$	$69.4^{+4.9+5.9}_{-4.9-5.8}$	97^{+1+18}_{-1-17}	$3.1^{+0.2+1.3}_{-0.2-1.2}$	254^{+13+20}_{-13-20}	286
56	350-500	1000+	3-4	2	$6.2^{+4.0+1.0}_{-3.6-1.0}$	$3.8^{+1.1+0.6}_{-1.0-0.6}$	$6.8^{+0.2+1.3}_{-0.2-1.3}$	$0.95^{+0.16+0.41}_{-0.16-0.36}$	$17.7^{+5.2+1.8}_{-4.6-1.8}$	25
57	500-750	500-1000	3-4	2	$11.8^{+3.3+2.0}_{-3.1-2.0}$	$10.5^{+1.8+1.6}_{-1.7-1.6}$	$39.7^{+0.5+7.4}_{-0.5-7.3}$	$0.22^{+0.04+0.09}_{-0.04-0.08}$	$62.1^{+5.1+7.8}_{-4.8-7.7}$	64
58	500-750	1000+	3-4	2	$2.6^{+2.3+0.6}_{-1.6-0.6}$	$2.9^{+1.5+0.6}_{-1.5-0.6}$	$4.90^{+0.21+0.92}_{-0.21-0.91}$	$0.10^{+0.03+0.04}_{-0.03-0.04}$	$10.5^{+3.8+1.2}_{-3.1-1.2}$	13
59	750+	750-1500	3-4	2	$0.0^{+1.1+0.0}_{-0.0-0.0}$	$0.32^{+0.48+0.09}_{-0.13-0.09}$	$6.3^{+0.2+1.4}_{-0.2-1.3}$	$0.03^{+0.02+0.01}_{-0.02-0.01}$	$6.6^{+1.6+1.4}_{-0.3-1.3}$	4
60	750+	1500+	3-4	2	$0.0^{+1.1+0.0}_{-0.0-0.0}$	$0.03^{+0.46+0.01}_{-0.02-0.01}$	$0.65^{+0.09+0.15}_{-0.08-0.14}$	$0.01^{+0.01+0.01}_{-0.01-0.00}$	$0.7^{+1.6+0.1}_{-0.1-0.1}$	1
61	300-350	300-500	3-4	3+	$6.4^{+2.8+0.7}_{-2.3-0.7}$	$10.3^{+1.9+2.7}_{-1.9-2.7}$	$5.0^{+0.0+2.8}_{-0.0-2.8}$	$0.35^{+0.18+0.42}_{-0.18-0.16}$	$22.0^{+4.7+3.9}_{-4.2-3.9}$	27
62	300-350	500-1000	3-4	3+	$4.9^{+2.7+0.6}_{-2.2-0.6}$	$6.2^{+1.4+1.7}_{-1.3-1.7}$	$2.5^{+0.0+1.4}_{-0.0-1.4}$	$0.75^{+0.52+0.90}_{-0.52-0.24}$	$14.4^{+4.2+2.4}_{-3.6-2.2}$	20
63	300-350	1000+	3-4	3+	$0.0^{+1.1+0.0}_{-0.0-0.0}$	$0.94^{+0.87+0.44}_{-0.74-0.44}$	$0.21^{+0.01+0.12}_{-0.01-0.12}$	$1.6^{+0.2+1.9}_{-0.2-1.4}$	$2.7^{+2.0+2.0}_{-0.8-1.5}$	4
64	350-500	350-500	3-4	3+	$0.6^{+1.2+0.1}_{-0.6-0.0}$	$4.2^{+1.5+1.3}_{-1.4-1.3}$	$2.5^{+0.0+1.4}_{-0.0-1.4}$	$0.09^{+0.04+0.11}_{-0.04-0.05}$	$7.4^{+2.6+1.9}_{-1.9-1.9}$	8
65	350-500	500-1000	3-4	3+	$10.2^{+6.3+2.1}_{-5.7-2.1}$	$7.0^{+1.5+1.9}_{-1.5-1.9}$	$4.3^{+0.0+2.4}_{-0.0-2.4}$	$0.78^{+0.18+0.94}_{-0.18-0.60}$	$22.3^{+7.9+3.8}_{-7.2-3.7}$	26
66	350-500	1000+	3-4	3+	$0.0^{+1.1+0.0}_{-0.0-0.0}$	$0.21^{+0.49+0.13}_{-0.16-0.13}$	$0.36^{+0.01+0.20}_{-0.01-0.20}$	$0.54^{+0.15+0.65}_{-0.15-0.39}$	$1.1^{+1.6+0.7}_{-0.2-0.5}$	5
67	500-750	500-1000	3-4	3+	$1.4^{+2.9+0.4}_{-1.4-0.0}$	$1.13^{+0.74+0.45}_{-0.58-0.45}$	$1.50^{+0.02+0.83}_{-0.02-0.83}$	$0.10^{+0.10+0.13}_{-0.10-0.00}$	$4.1^{+3.6+1.0}_{-2.0-0.9}$	0
68	500-750	1000+	3-4	3+	$0.00^{+0.95+0.00}_{-0.00-0.00}$	$0.12^{+0.46+0.09}_{-0.06-0.09}$	$0.26^{+0.01+0.15}_{-0.01-0.15}$	$0.02^{+0.03+0.02}_{-0.02-0.00}$	$0.4^{+1.4+0.2}_{-0.1-0.2}$	2
69	750+	750-1500	3-4	3+	$0.00^{+0.97+0.00}_{-0.00-0.00}$	$0.00^{+0.46+0.00}_{-0.00-0.00}$	$0.29^{+0.01+0.16}_{-0.01-0.16}$	$0.01^{+0.02+0.01}_{-0.01-0.00}$	$0.3^{+1.4+0.2}_{-0.0-0.2}$	1
70	750+	1500+	3-4	3+	$0.0^{+1.4+0.0}_{-0.0-0.0}$	$0.00^{+0.46+0.00}_{-0.00-0.00}$	$0.04^{+0.01+0.02}_{-0.00-0.02}$	$0.01^{+0.03+0.02}_{-0.01-0.00}$	$0.0^{+1.8+0.0}_{-0.0-0.0}$	0

Table B.3: Observed number of events and pre-fit background predictions in the $5 \leq N_{\text{jet}} \leq 6$ search bins.

Bin	$H_{\text{T}}^{\text{miss}}$ [GeV]	H_{T} [GeV]	N_{jet}	$N_{\text{b-jet}}$	Lost-e/μ	$\tau \to$ had	$Z \to \nu\bar{\nu}$	QCD	Total Pred.	Obs.
71	300-350	300-500	5-6	0	217^{+11+22}_{-11-22}	166^{+6+27}_{-6-27}	489^{+12+42}_{-12-39}	49^{+5+21}_{-5-19}	922^{+21+58}_{-21-56}	1015
72	300-350	500-1000	5-6	0	397^{+13+37}_{-13-37}	403^{+9+36}_{-9-36}	772^{+16+61}_{-15-57}	113^{+4+47}_{-4-43}	1686^{+27+93}_{-27-88}	1673
73	300-350	1000+	5-6	0	$49.6^{+4.5+5.4}_{-4.5-5.4}$	$55.1^{+3.8+8.3}_{-3.8-8.3}$	$100.0^{+6.4+8.2}_{-6.0-7.1}$	49^{+1+21}_{-1-19}	254^{+11+24}_{-10-22}	226
74	350-500	350-500	5-6	0	71^{+7+11}_{-6-11}	47^{+3+16}_{-3-16}	242^{+9+20}_{-9-19}	$12.7^{+2.3+5.3}_{-2.3-4.8}$	372^{+13+29}_{-13-28}	464
75	350-500	500-1000	5-6	0	384^{+12+33}_{-12-33}	412^{+11+32}_{-11-32}	1110^{+19+84}_{-19-78}	65^{+2+27}_{-2-25}	1971^{+30+99}_{-29-93}	2018
76	350-500	1000+	5-6	0	$76.9^{+6.4+8.9}_{-6.4-8.9}$	$72.4^{+4.8+9.3}_{-4.8-9.3}$	170^{+8+14}_{-8-12}	28^{+1+12}_{-1-11}	347^{+14+22}_{-14-21}	320
77	500-750	500-1000	5-6	0	$66.7^{+5.1+7.3}_{-5.0-7.3}$	$70.1^{+4.3+6.1}_{-4.2-6.0}$	302^{+10+23}_{-10-22}	$3.2^{+0.1+1.3}_{-0.1-1.2}$	442^{+14+25}_{-14-24}	460
78	500-750	1000+	5-6	0	$23.9^{+2.9+4.5}_{-2.9-4.5}$	$31.2^{+3.1+4.0}_{-3.1-4.0}$	$123.5^{+7.3+9.4}_{-6.9-8.9}$	$2.5^{+0.1+1.1}_{-0.1-1.0}$	181^{+10+11}_{-9-11}	170
79	750+	750-1500	5-6	0	$4.0^{+1.2+0.7}_{-1.1-0.7}$	$4.90^{+0.89+0.52}_{-0.76-0.52}$	$52.2^{+4.6+7.5}_{-4.2-6.8}$	$0.23^{+0.04+0.10}_{-0.04-0.09}$	$61.3^{+5.0+7.5}_{-4.6-6.9}$	74
80	750+	1500+	5-6	0	$0.90^{+0.61+0.19}_{-0.45-0.19}$	$1.46^{+0.67+0.16}_{-0.49-0.16}$	$16.5^{+2.9+2.7}_{-2.5-2.5}$	$0.25^{+0.06+0.11}_{-0.06-0.10}$	$19.1^{+3.2+2.7}_{-2.7-2.5}$	19
81	300-350	300-500	5-6	1	130^{+8+11}_{-8-11}	131^{+6+17}_{-6-17}	133^{+3+19}_{-3-19}	$12.8^{+2.8+5.2}_{-2.8-4.9}$	407^{+15+29}_{-15-28}	450
82	300-350	500-1000	5-6	1	290^{+11+25}_{-11-25}	302^{+8+25}_{-8-25}	218^{+4+31}_{-4-30}	41^{+4+17}_{-4-16}	851^{+20+50}_{-20-49}	781
83	300-350	1000+	5-6	1	$25.8^{+3.4+2.5}_{-3.4-2.5}$	$31.6^{+2.9+5.9}_{-2.9-5.9}$	$29.0^{+1.8+4.1}_{-1.7-4.0}$	$18.4^{+0.8+7.5}_{-0.8-7.1}$	105^{+7+11}_{-6-10}	100
84	350-500	350-500	5-6	1	$45.4^{+5.5+5.4}_{-5.4-5.4}$	32^{+3+11}_{-3-11}	$65.1^{+2.4+9.3}_{-2.3-9.1}$	$3.7^{+0.5+1.5}_{-0.5-1.4}$	146^{+9+16}_{-8-16}	160
85	350-500	500-1000	5-6	1	228^{+10+20}_{-10-20}	269^{+8+21}_{-8-21}	310^{+5+43}_{-5-42}	28^{+3+11}_{-3-11}	834^{+19+53}_{-19-52}	801
86	350-500	1000+	5-6	1	$40.5^{+5.5+4.2}_{-5.4-4.2}$	$36.0^{+3.3+4.3}_{-3.3-4.2}$	$49.4^{+2.3+7.0}_{-2.2-6.7}$	$11.9^{+0.7+4.8}_{-0.7-4.5}$	138^{+9+10}_{-9-10}	138
87	500-750	500-1000	5-6	1	$23.4^{+3.5+2.6}_{-3.4-2.6}$	$32.1^{+2.8+3.3}_{-2.8-3.3}$	84^{+3+12}_{-3-12}	$1.45^{+0.11+0.59}_{-0.11-0.55}$	141^{+7+13}_{-7-12}	135
88	500-750	1000+	5-6	1	$8.5^{+1.8+1.1}_{-1.7-1.1}$	$13.0^{+1.8+1.5}_{-1.7-1.5}$	$35.3^{+2.1+4.9}_{-2.0-4.8}$	$1.33^{+0.17+0.54}_{-0.17-0.51}$	$58.0^{+4.1+5.3}_{-3.9-5.2}$	49
89	750+	750-1500	5-6	1	$3.7^{+1.4+0.7}_{-1.2-0.7}$	$2.9^{+1.0+0.4}_{-0.9-0.4}$	$14.9^{+1.3+2.8}_{-1.2-2.6}$	$0.07^{+0.01+0.03}_{-0.01-0.03}$	$21.6^{+2.8+2.9}_{-2.5-2.7}$	16
90	750+	1500+	5-6	1	$1.06^{+0.74+0.26}_{-0.56-0.26}$	$1.16^{+0.73+0.18}_{-0.57-0.18}$	$4.79^{+0.85+0.96}_{-0.73-0.92}$	$0.16^{+0.07+0.07}_{-0.07-0.06}$	$7.2^{+1.7+1.0}_{-1.3-1.0}$	6
91	300-350	300-500	5-6	2	$60.1^{+7.1+6.0}_{-7.0-6.0}$	$50.2^{+3.3+4.9}_{-3.3-4.9}$	$23.8^{+0.6+7.1}_{-0.6-7.1}$	$2.9^{+0.9+1.1}_{-0.9-1.1}$	137^{+10+11}_{-10-11}	143
92	300-350	500-1000	5-6	2	137^{+9+13}_{-9-13}	160^{+6+14}_{-6-14}	39^{+1+12}_{-1-11}	$11.8^{+1.8+4.6}_{-1.8-4.5}$	347^{+15+22}_{-15-22}	332
93	300-350	1000+	5-6	2	$16.9^{+3.8+2.0}_{-3.7-2.0}$	$15.9^{+2.1+2.1}_{-2.1-2.1}$	$5.1^{+0.3+1.5}_{-0.3-1.5}$	$5.6^{+0.4+2.2}_{-0.4-2.2}$	$43.5^{+5.9+3.9}_{-5.8-3.9}$	36
94	350-500	350-500	5-6	2	$13.3^{+3.1+1.9}_{-2.9-1.9}$	$7.0^{+1.1+2.3}_{-1.0-2.3}$	$11.7^{+0.4+3.5}_{-0.4-3.5}$	$1.02^{+0.54+0.40}_{-0.54-0.39}$	$32.9^{+4.3+4.6}_{-4.0-4.6}$	28
95	350-500	500-1000	5-6	2	$107.5^{+7.6+9.6}_{-7.6-9.6}$	$121.2^{+5.8+9.9}_{-5.8-9.8}$	55^{+1+16}_{-1-16}	$5.9^{+1.0+2.3}_{-1.0-2.2}$	290^{+14+22}_{-13-21}	288
96	350-500	1000+	5-6	2	$14.2^{+2.8+1.8}_{-2.7-1.8}$	$15.7^{+2.2+2.0}_{-2.1-2.0}$	$8.7^{+0.4+2.6}_{-0.4-2.6}$	$3.2^{+0.1+1.2}_{-0.1-1.2}$	$41.8^{+5.0+4.0}_{-4.8-3.9}$	44
97	500-750	500-1000	5-6	2	$8.4^{+2.3+1.1}_{-2.2-1.1}$	$8.3^{+1.3+1.0}_{-1.2-1.0}$	$15.0^{+0.5+4.4}_{-0.5-4.4}$	$0.34^{+0.05+0.13}_{-0.05-0.13}$	$32.1^{+3.7+4.7}_{-3.4-4.7}$	35
98	500-750	1000+	5-6	2	$2.1^{+1.3+0.3}_{-1.0-0.3}$	$4.0^{+1.1+0.6}_{-1.0-0.6}$	$6.2^{+0.4+1.9}_{-0.3-1.8}$	$0.16^{+0.05+0.06}_{-0.05-0.06}$	$12.5^{+2.4+2.0}_{-2.0-2.0}$	18
99	750+	750-1500	5-6	2	$0.74^{+0.87+0.22}_{-0.53-0.22}$	$0.68^{+0.64+0.16}_{-0.45-0.16}$	$2.64^{+0.23+0.85}_{-0.21-0.83}$	$0.05^{+0.05+0.02}_{-0.05-0.00}$	$4.1^{+1.5+0.9}_{-1.0-0.9}$	8
100	750+	1500+	5-6	2	$0.77^{+0.65+0.24}_{-0.45-0.24}$	$1.07^{+0.72+0.33}_{-0.56-0.33}$	$0.84^{+0.15+0.28}_{-0.13-0.27}$	$0.03^{+0.03+0.01}_{-0.03-0.00}$	$2.7^{+1.4+0.5}_{-1.0-0.5}$	3
101	300-350	300-500	5-6	3+	$2.8^{+1.5+0.3}_{-1.2-0.3}$	$5.1^{+1.0+0.8}_{-0.9-0.8}$	$2.0^{+0.0+1.1}_{-0.0-1.1}$	$0.50^{+0.37+0.57}_{-0.37-0.13}$	$10.4^{+2.5+1.5}_{-2.1-1.4}$	18
102	300-350	500-1000	5-6	3+	$17.0^{+3.2+1.6}_{-3.1-1.6}$	$23.5^{+2.4+3.2}_{-2.3-3.2}$	$4.2^{+0.1+2.3}_{-0.1-2.3}$	$3.9^{+2.3+4.5}_{-2.3-1.6}$	$48.7^{+6.0+6.2}_{-5.9-4.5}$	44
103	300-350	1000+	5-6	3+	$4.4^{+2.1+0.6}_{-1.8-0.6}$	$2.50^{+0.86+0.47}_{-0.73-0.47}$	$0.65^{+0.04+0.35}_{-0.04-0.35}$	$3.3^{+0.4+3.7}_{-0.4-2.8}$	$10.8^{+3.0+3.8}_{-2.6-3.0}$	6
104	350-500	350-500	5-6	3+	$0.8^{+1.7+0.2}_{-0.8-0.0}$	$1.14^{+0.75+0.33}_{-0.59-0.33}$	$0.87^{+0.03+0.47}_{-0.03-0.47}$	$0.18^{+0.08+0.21}_{-0.08-0.10}$	$3.0^{+2.4+0.6}_{-1.4-0.6}$	4
105	350-500	500-1000	5-6	3+	$15.2^{+2.6+1.5}_{-2.6-1.5}$	$17.6^{+2.2+2.7}_{-2.1-2.7}$	$5.7^{+0.1+3.1}_{-0.1-3.1}$	$1.7^{+0.1+1.9}_{-0.1-1.6}$	$40.2^{+4.8+4.8}_{-4.7-4.6}$	34
106	350-500	1000+	5-6	3+	$1.9^{+1.1+0.3}_{-0.8-0.3}$	$3.8^{+1.1+0.7}_{-1.0-0.7}$	$1.14^{+0.05+0.62}_{-0.05-0.62}$	$2.4^{+0.3+2.7}_{-0.3-2.1}$	$9.2^{+2.2+2.8}_{-1.9-2.3}$	8
107	500-750	500-1000	5-6	3+	$1.8^{+1.1+0.3}_{-0.8-0.3}$	$1.71^{+0.77+0.67}_{-0.61-0.67}$	$1.48^{+0.05+0.81}_{-0.05-0.80}$	$0.20^{+0.04+0.23}_{-0.04-0.17}$	$5.2^{+1.8+1.1}_{-1.5-1.1}$	4
108	500-750	1000+	5-6	3+	$1.13^{+0.96+0.25}_{-0.66-0.25}$	$0.94^{+0.67+0.27}_{-0.49-0.27}$	$0.73^{+0.04+0.40}_{-0.04-0.40}$	$0.11^{+0.03+0.12}_{-0.03-0.08}$	$2.9^{+1.6+0.6}_{-1.1-0.6}$	2
109	750+	750-1500	5-6	3+	$0.00^{+0.72+0.00}_{-0.00-0.00}$	$0.07^{+0.46+0.04}_{-0.06-0.04}$	$0.31^{+0.03+0.17}_{-0.03-0.17}$	$0.02^{+0.04+0.03}_{-0.02-0.00}$	$0.4^{+1.2+0.2}_{-0.1-0.2}$	0
110	750+	1500+	5-6	3+	$0.00^{+0.63+0.00}_{-0.00-0.00}$	$0.03^{+0.46+0.01}_{-0.02-0.01}$	$0.11^{+0.02+0.06}_{-0.02-0.06}$	$0.00^{+0.02+0.01}_{-0.00-0.00}$	$0.1^{+1.1+0.1}_{-0.0-0.1}$	1

Table B.4: Observed number of events and pre-fit background predictions in the $7 \leq N_{\text{jet}} \leq 8$ search bins.

Bin	$H_{\text{T}}^{\text{miss}}$ [GeV]	H_{T} [GeV]	N_{jet}	$N_{\text{b-jet}}$	Lost-e/μ	$\tau \to$ had	$Z \to \nu\bar{\nu}$	QCD	Total Pred.	Obs.
111	300-350	500-1000	7-8	0	$48.0^{+3.9+5.4}_{-3.8-5.4}$	$60.8^{+3.4+6.0}_{-3.4-6.0}$	76^{+5+11}_{-5-10}	30^{+2+12}_{-2-11}	215^{+9+18}_{-9-17}	218
112	300-350	1000+	7-8	0	$21.2^{+2.9+2.3}_{-2.9-2.3}$	$20.3^{+2.2+2.8}_{-2.1-2.8}$	$23.9^{+3.3+2.8}_{-2.9-2.5}$	$20.5^{+0.5+8.5}_{-0.5-7.8}$	$85.9^{+6.1+9.6}_{-5.8-9.0}$	85
113	350-500	500-1000	7-8	0	$43.2^{+3.9+4.9}_{-3.9-4.9}$	$54.2^{+3.6+5.7}_{-3.5-5.7}$	89^{+6+11}_{-5-10}	$14.3^{+1.9+5.9}_{-1.9-5.4}$	201^{+10+14}_{-9-14}	215
114	350-500	1000+	7-8	0	$22.5^{+2.8+2.7}_{-2.7-2.7}$	$23.3^{+2.5+2.3}_{-2.4-2.3}$	$48.3^{+4.7+5.4}_{-4.3-4.8}$	$12.6^{+0.7+5.2}_{-0.7-4.8}$	$106.7^{+7.1+8.3}_{-6.7-7.7}$	75
115	500-750	500-1000	7-8	0	$6.9^{+1.8+1.4}_{-1.7-1.4}$	$4.96^{+0.95+0.77}_{-0.84-0.77}$	$26.5^{+3.6+3.3}_{-3.2-3.0}$	$0.88^{+0.10+0.36}_{-0.10-0.34}$	$39.2^{+4.5+3.7}_{-4.1-3.5}$	34
116	500-750	1000+	7-8	0	$5.4^{+1.1+0.9}_{-1.0-0.9}$	$9.9^{+1.6+1.7}_{-1.5-1.7}$	$27.2^{+3.7+3.1}_{-3.2-2.8}$	$1.56^{+0.12+0.64}_{-0.12-0.59}$	$44.1^{+4.5+3.7}_{-4.1-3.5}$	38
117	750+	750-1500	7-8	0	$1.26^{+0.70+0.50}_{-0.58-0.50}$	$1.44^{+0.74+0.24}_{-0.57-0.24}$	$3.6^{+1.4+0.7}_{-1.0-0.6}$	$0.07^{+0.02+0.03}_{-0.02-0.03}$	$6.4^{+2.0+0.9}_{-1.5-0.8}$	5
118	750+	1500+	7-8	0	$0.69^{+0.47+0.16}_{-0.35-0.16}$	$1.03^{+0.69+0.15}_{-0.51-0.15}$	$1.5^{+1.2+0.3}_{-0.7-0.3}$	$0.07^{+0.01+0.03}_{-0.01-0.03}$	$3.3^{+1.7+0.4}_{-1.1-0.4}$	5
119	300-350	500-1000	7-8	1	$64.7^{+5.1+6.4}_{-5.1-6.4}$	$77.0^{+3.9+7.5}_{-3.8-7.4}$	$31.7^{+2.1+8.6}_{-1.9-8.4}$	$11.2^{+0.5+4.7}_{-0.5-4.3}$	184^{+9+14}_{-9-14}	146
120	300-350	1000+	7-8	1	$16.3^{+2.4+1.7}_{-2.4-1.7}$	$19.9^{+2.2+2.1}_{-2.1-2.1}$	$10.3^{+1.4+2.7}_{-1.2-2.6}$	$8.3^{+0.2+3.5}_{-0.2-3.2}$	$54.8^{+4.8+5.2}_{-4.7-5.0}$	68
121	350-500	500-1000	7-8	1	$46.9^{+4.4+5.0}_{-4.4-5.0}$	$58.6^{+3.7+5.7}_{-3.7-5.7}$	$37.0^{+2.4+9.7}_{-2.2-9.5}$	$7.5^{+0.4+3.2}_{-0.4-2.9}$	150^{+8+13}_{-8-12}	113
122	350-500	1000+	7-8	1	$19.5^{+2.5+2.1}_{-2.4-2.1}$	$19.5^{+2.3+2.0}_{-2.3-2.0}$	$21.0^{+2.0+5.4}_{-1.9-5.3}$	$5.3^{+0.5+2.2}_{-0.5-2.0}$	$65.3^{+5.2+6.5}_{-5.1-6.4}$	67
123	500-750	500-1000	7-8	1	$7.6^{+2.0+1.4}_{-1.9-1.4}$	$5.5^{+1.1+0.8}_{-1.1-0.8}$	$11.5^{+1.6+3.0}_{-1.4-3.0}$	$0.36^{+0.04+0.15}_{-0.04-0.14}$	$24.9^{+3.5+3.4}_{-3.3-3.4}$	19
124	500-750	1000+	7-8	1	$9.3^{+2.1+1.3}_{-2.0-1.3}$	$7.5^{+1.5+0.8}_{-1.4-0.8}$	$11.4^{+1.5+3.0}_{-1.4-2.9}$	$0.98^{+0.12+0.41}_{-0.12-0.37}$	$29.2^{+3.9+3.3}_{-3.7-3.3}$	22
125	750+	750-1500	7-8	1	$0.14^{+0.30+0.05}_{-0.14-0.00}$	$0.44^{+0.51+0.10}_{-0.22-0.10}$	$1.48^{+0.56+0.44}_{-0.42-0.43}$	$0.07^{+0.03+0.03}_{-0.03-0.03}$	$2.14^{+0.99+0.46}_{-0.56-0.45}$	4
126	750+	1500+	7-8	1	$0.00^{+0.47+0.00}_{-0.00-0.00}$	$0.14^{+0.47+0.02}_{-0.08-0.02}$	$0.70^{+0.55+0.22}_{-0.34-0.21}$	$0.03^{+0.01+0.01}_{-0.01-0.01}$	$0.9^{+1.1+0.2}_{-0.3-0.2}$	6
127	300-350	500-1000	7-8	2	$34.7^{+3.5+3.6}_{-3.5-3.6}$	$47.7^{+3.0+4.4}_{-3.0-4.4}$	$8.1^{+0.5+3.6}_{-0.5-3.5}$	$5.3^{+0.5+2.1}_{-0.5-2.1}$	$95.8^{+6.6+7.1}_{-6.5-7.0}$	95
128	300-350	1000+	7-8	2	$9.0^{+2.1+1.2}_{-2.1-1.2}$	$10.8^{+1.4+1.3}_{-1.4-1.3}$	$2.4^{+0.3+1.0}_{-0.3-1.0}$	$3.2^{+0.1+1.3}_{-0.1-1.3}$	$25.4^{+3.6+2.4}_{-3.4-2.4}$	26
129	350-500	500-1000	7-8	2	$26.2^{+3.0+2.9}_{-3.0-2.9}$	$31.0^{+2.5+3.3}_{-2.5-3.2}$	$9.6^{+0.6+4.1}_{-0.6-4.1}$	$2.5^{+0.2+1.0}_{-0.2-1.0}$	$69.3^{+5.6+6.1}_{-5.5-6.1}$	84
130	350-500	1000+	7-8	2	$13.3^{+2.5+1.5}_{-2.4-1.5}$	$13.3^{+1.8+1.3}_{-1.7-1.3}$	$4.7^{+0.5+2.0}_{-0.4-2.0}$	$1.95^{+0.13+0.78}_{-0.13-0.75}$	$33.3^{+4.3+3.0}_{-4.2-2.9}$	35
131	500-750	500-1000	7-8	2	$2.5^{+1.4+0.5}_{-1.2-0.5}$	$0.86^{+0.50+0.21}_{-0.18-0.21}$	$2.6^{+0.3+1.1}_{-0.3-1.1}$	$0.10^{+0.01+0.04}_{-0.01-0.04}$	$6.0^{+1.9+1.3}_{-1.4-1.3}$	7
132	500-750	1000+	7-8	2	$6.0^{+2.3+1.0}_{-2.2-1.0}$	$3.3^{+1.0+0.6}_{-0.9-0.6}$	$2.9^{+0.4+1.2}_{-0.3-1.2}$	$0.22^{+0.06+0.09}_{-0.06-0.08}$	$12.4^{+3.4+1.7}_{-3.1-1.7}$	12
133	750+	750-1500	7-8	2	$0.16^{+0.34+0.08}_{-0.16-0.00}$	$0.44^{+0.56+0.15}_{-0.32-0.15}$	$0.39^{+0.15+0.18}_{-0.11-0.18}$	$0.03^{+0.01+0.01}_{-0.01-0.01}$	$1.03^{+0.91+0.25}_{-0.49-0.23}$	2
134	750+	1500+	7-8	2	$0.53^{+0.62+0.20}_{-0.38-0.20}$	$0.61^{+0.57+0.22}_{-0.33-0.22}$	$0.13^{+0.10+0.06}_{-0.06-0.06}$	$0.06^{+0.02+0.02}_{-0.02-0.02}$	$1.3^{+1.2+0.3}_{-0.7-0.3}$	2
135	300-350	500-1000	7-8	3+	$8.1^{+1.8+1.0}_{-1.7-1.0}$	$9.4^{+1.4+1.3}_{-1.3-1.3}$	$4.1^{+0.3+2.3}_{-0.2-2.3}$	$2.9^{+0.6+3.3}_{-0.6-2.3}$	$24.6^{+3.2+4.3}_{-3.1-3.7}$	12
136	300-350	1000+	7-8	3+	$4.7^{+2.0+0.7}_{-1.8-0.7}$	$5.4^{+1.2+0.8}_{-1.1-0.8}$	$1.51^{+0.21+0.85}_{-0.18-0.84}$	$2.4^{+0.3+2.7}_{-0.3-2.1}$	$13.9^{+3.2+3.0}_{-2.9-2.5}$	8
137	350-500	500-1000	7-8	3+	$5.9^{+1.9+0.8}_{-1.7-0.8}$	$7.4^{+1.4+1.2}_{-1.3-1.2}$	$4.7^{+0.3+2.7}_{-0.3-2.7}$	$1.2^{+0.1+1.3}_{-0.1-1.1}$	$19.2^{+3.2+3.3}_{-3.1-3.2}$	16
138	350-500	1000+	7-8	3+	$2.6^{+1.1+0.3}_{-1.0-0.3}$	$4.8^{+1.3+0.7}_{-1.2-0.7}$	$3.1^{+0.3+1.8}_{-0.3-1.8}$	$2.1^{+0.3+2.3}_{-0.3-1.8}$	$12.6^{+2.5+3.0}_{-2.2-2.6}$	8
139	500-750	500-1000	7-8	3+	$0.23^{+0.48+0.08}_{-0.23-0.00}$	$0.30^{+0.48+0.10}_{-0.13-0.10}$	$1.70^{+0.23+0.96}_{-0.20-0.96}$	$0.11^{+0.04+0.12}_{-0.04-0.08}$	$2.34^{+0.99+0.98}_{-0.41-0.96}$	3
140	500-750	1000+	7-8	3+	$3.4^{+2.4+0.7}_{-2.1-0.7}$	$1.59^{+0.83+0.49}_{-0.69-0.49}$	$1.51^{+0.20+0.85}_{-0.18-0.85}$	$0.22^{+0.08+0.24}_{-0.08-0.14}$	$6.7^{+3.2+1.2}_{-2.7-1.2}$	4
141	750+	750-1500	7-8	3+	$0.00^{+0.56+0.00}_{-0.00-0.00}$	$0.05^{+0.46+0.02}_{-0.03-0.02}$	$0.19^{+0.07+0.11}_{-0.05-0.11}$	$0.03^{+0.04+0.03}_{-0.03-0.00}$	$0.3^{+1.0+0.1}_{-0.1-0.1}$	0
142	750+	1500+	7-8	3+	$0.00^{+0.72+0.00}_{-0.00-0.00}$	$0.04^{+0.46+0.02}_{-0.02-0.02}$	$0.12^{+0.10+0.07}_{-0.06-0.07}$	$0.01^{+0.03+0.01}_{-0.01-0.00}$	$0.2^{+1.2+0.1}_{-0.1-0.1}$	0

Table B.5: Observed number of events and pre-fit background predictions in the $N_{\text{jet}} \geq 9$ search bins.

Bin	$H_{\text{T}}^{\text{miss}}$ [GeV]	H_{T} [GeV]	N_{jet}	$N_{\text{b-jet}}$	Lost-e/μ	$\tau \to$ had	$Z \to \nu\bar{\nu}$	QCD	Total Pred.	Obs.
143	300-350	500-1000	9+	0	$6.2^{+2.7+1.7}_{-2.6-1.7}$	$3.46^{+0.89+0.59}_{-0.77-0.59}$	$2.6^{+1.2+0.7}_{-0.9-0.7}$	$2.9^{+0.3+1.3}_{-0.3-1.1}$	$15.1^{+3.8+2.3}_{-3.5-2.2}$	7
144	300-350	1000+	9+	0	$3.5^{+1.2+0.6}_{-1.1-0.6}$	$4.6^{+1.0+0.6}_{-0.9-0.6}$	$3.0^{+1.4+0.6}_{-1.0-0.6}$	$4.2^{+0.3+1.9}_{-0.3-1.6}$	$15.2^{+2.7+2.1}_{-2.3-1.9}$	12
145	350-500	500-1000	9+	0	$2.39^{+0.99+0.69}_{-0.89-0.69}$	$2.39^{+0.86+0.48}_{-0.73-0.48}$	$2.9^{+1.3+0.7}_{-0.9-0.6}$	$0.97^{+0.08+0.43}_{-0.08-0.37}$	$8.6^{+2.3+1.2}_{-1.9-1.1}$	6
146	350-500	1000+	9+	0	$3.7^{+1.1+0.6}_{-1.1-0.6}$	$4.6^{+1.0+0.6}_{-0.9-0.6}$	$5.5^{+1.9+1.0}_{-1.5-0.9}$	$3.1^{+0.2+1.4}_{-0.2-1.2}$	$17.0^{+2.9+1.9}_{-2.5-1.7}$	13
147	500-750	500-1000	9+	0	$0.15^{+0.32+0.10}_{-0.15-0.00}$	$0.35^{+0.55+0.12}_{-0.30-0.12}$	$1.0^{+1.3+0.4}_{-0.7-0.4}$	$0.10^{+0.05+0.04}_{-0.05-0.04}$	$1.6^{+1.6+0.5}_{-0.8-0.4}$	2
148	500-750	1000+	9+	0	$0.98^{+0.50+0.26}_{-0.41-0.26}$	$1.98^{+0.74+0.30}_{-0.58-0.30}$	$3.5^{+1.6+0.7}_{-1.1-0.7}$	$0.47^{+0.05+0.21}_{-0.05-0.18}$	$6.9^{+2.0+0.8}_{-1.5-0.8}$	11
149	750+	750-1500	9+	0	$0.00^{+0.44+0.00}_{-0.00-0.00}$	$0.00^{+0.46+0.00}_{-0.00-0.00}$	$0.00^{+0.64+0.00}_{-0.00-0.00}$	$0.01^{+0.02+0.00}_{-0.01-0.00}$	$0.0^{+1.1+0.0}_{-0.0-0.0}$	0
150	750+	1500+	9+	0	$0.23^{+0.27+0.16}_{-0.17-0.16}$	$0.28^{+0.50+0.08}_{-0.21-0.08}$	$0.00^{+0.82+0.00}_{-0.00-0.00}$	$0.05^{+0.03+0.02}_{-0.03-0.02}$	$0.6^{+1.1+0.2}_{-0.4-0.2}$	1
151	300-350	500-1000	9+	1	$6.5^{+1.8+1.1}_{-1.7-1.1}$	$4.57^{+0.93+0.77}_{-0.81-0.77}$	$1.83^{+0.84+0.68}_{-0.60-0.74}$	$1.02^{+0.06+0.42}_{-0.06-0.40}$	$13.9^{+2.8+1.5}_{-2.6-1.6}$	25
152	300-350	1000+	9+	1	$5.7^{+1.6+0.7}_{-1.5-0.7}$	$7.3^{+1.3+1.1}_{-1.2-1.1}$	$2.08^{+0.95+0.69}_{-0.68-0.77}$	$2.43^{+0.06+0.99}_{-0.06-0.94}$	$17.5^{+3.0+1.8}_{-2.8-1.8}$	20
153	350-500	500-1000	9+	1	$2.92^{+0.94+0.57}_{-0.84-0.57}$	$2.96^{+0.77+0.60}_{-0.61-0.60}$	$2.00^{+0.91+0.71}_{-0.65-0.78}$	$0.53^{+0.05+0.22}_{-0.05-0.21}$	$8.4^{+1.9+1.1}_{-1.6-1.2}$	8
154	350-500	1000+	9+	1	$5.4^{+1.4+0.7}_{-1.3-0.7}$	$7.7^{+1.4+1.1}_{-1.3-1.1}$	$3.9^{+1.3+1.3}_{-1.0-1.4}$	$1.48^{+0.05+0.60}_{-0.05-0.57}$	$18.4^{+3.1+1.9}_{-2.8-2.0}$	14
155	500-750	500-1000	9+	1	$0.14^{+0.30+0.08}_{-0.14-0.00}$	$0.24^{+0.49+0.21}_{-0.18-0.16}$	$0.71^{+0.94+0.35}_{-0.46-0.36}$	$0.03^{+0.03+0.01}_{-0.03-0.00}$	$1.1^{+1.2+0.4}_{-0.6-0.4}$	1
156	500-750	1000+	9+	1	$0.68^{+0.58+0.12}_{-0.41-0.12}$	$1.20^{+0.64+0.21}_{-0.44-0.21}$	$2.4^{+1.1+0.8}_{-0.8-0.9}$	$0.20^{+0.02+0.08}_{-0.02-0.07}$	$4.5^{+1.6+0.8}_{-1.2-0.9}$	4
157	750+	750-1500	9+	1	$0.00^{+0.73+0.00}_{-0.00-0.00}$	$0.04^{+0.46+0.02}_{-0.04-0.00}$	$0.00^{+0.45+0.00}_{-0.00-0.00}$	$0.01^{+0.01+0.00}_{-0.01-0.00}$	$0.1^{+1.3+0.0}_{-0.0-0.0}$	0
158	750+	1500+	9+	1	$0.13^{+0.27+0.06}_{-0.13-0.00}$	$0.03^{+0.46+0.01}_{-0.02-0.01}$	$0.00^{+0.57+0.00}_{-0.00-0.00}$	$0.02^{+0.01+0.01}_{-0.01-0.01}$	$0.18^{+0.93+0.06}_{-0.15-0.01}$	0
159	300-350	500-1000	9+	2	$4.1^{+1.3+0.7}_{-1.2-0.7}$	$4.68^{+0.92+0.85}_{-0.80-0.85}$	$0.64^{+0.29+0.34}_{-0.21-0.36}$	$0.40^{+0.06+0.24}_{-0.06-0.21}$	$9.8^{+2.2+1.2}_{-2.0-1.2}$	13
160	300-350	1000+	9+	2	$5.2^{+1.6+0.7}_{-1.5-0.7}$	$5.5^{+1.2+1.0}_{-1.1-1.0}$	$0.73^{+0.33+0.37}_{-0.24-0.39}$	$1.32^{+0.15+0.68}_{-0.15-0.58}$	$12.7^{+2.8+1.4}_{-2.6-1.4}$	10
161	350-500	500-1000	9+	2	$3.01^{+0.91+0.63}_{-0.82-0.63}$	$4.7^{+1.1+0.9}_{-1.0-0.9}$	$0.70^{+0.32+0.36}_{-0.23-0.39}$	$0.30^{+0.08+0.14}_{-0.08-0.12}$	$8.7^{+2.0+1.1}_{-1.8-1.1}$	4
162	350-500	1000+	9+	2	$4.4^{+1.1+0.6}_{-1.1-0.6}$	$6.3^{+1.4+0.8}_{-1.3-0.8}$	$1.35^{+0.47+0.67}_{-0.36-0.72}$	$0.63^{+0.03+0.32}_{-0.03-0.27}$	$12.7^{+2.6+1.3}_{-2.4-1.3}$	12
163	500-750	500-1000	9+	2	$0.00^{+0.39+0.00}_{-0.00-0.00}$	$0.35^{+0.49+0.17}_{-0.18-0.17}$	$0.25^{+0.33+0.15}_{-0.16-0.16}$	$0.01^{+0.01+0.01}_{-0.01-0.00}$	$0.61^{+0.95+0.23}_{-0.24-0.23}$	0
164	500-750	1000+	9+	2	$2.0^{+1.1+0.4}_{-0.9-0.4}$	$1.95^{+0.87+0.45}_{-0.73-0.45}$	$0.84^{+0.39+0.43}_{-0.28-0.46}$	$0.09^{+0.02+0.04}_{-0.02-0.04}$	$4.9^{+2.0+0.7}_{-1.7-0.7}$	7
165	750+	750-1500	9+	2	$0.00^{+0.60+0.00}_{-0.00-0.00}$	$0.01^{+0.46+0.01}_{-0.00-0.00}$	$0.00^{+0.16+0.00}_{-0.00-0.00}$	$0.00^{+0.01+0.00}_{-0.00-0.00}$	$0.0^{+1.1+0.0}_{-0.0-0.0}$	0
166	750+	1500+	9+	2	$0.00^{+0.38+0.00}_{-0.00-0.00}$	$0.00^{+0.46+0.00}_{-0.00-0.00}$	$0.00^{+0.20+0.00}_{-0.00-0.00}$	$0.01^{+0.02+0.00}_{-0.01-0.00}$	$0.01^{+0.87+0.00}_{-0.01-0.00}$	0
167	300-350	500-1000	9+	3+	$1.06^{+0.63+0.27}_{-0.50-0.27}$	$1.06^{+0.57+0.29}_{-0.34-0.29}$	$0.37^{+0.17+0.26}_{-0.12-0.28}$	$0.47^{+0.13+0.56}_{-0.13-0.34}$	$3.0^{+1.2+0.7}_{-0.9-0.6}$	1
168	300-350	1000+	9+	3+	$3.5^{+1.7+0.5}_{-1.5-0.5}$	$2.6^{+1.0+0.7}_{-0.9-0.7}$	$0.42^{+0.19+0.29}_{-0.14-0.31}$	$2.1^{+0.3+2.4}_{-0.3-1.8}$	$8.6^{+2.7+2.6}_{-2.4-2.0}$	4
169	350-500	500-1000	9+	3+	$1.03^{+0.60+0.30}_{-0.47-0.30}$	$1.58^{+0.71+0.43}_{-0.55-0.43}$	$0.40^{+0.18+0.28}_{-0.13-0.31}$	$0.10^{+0.03+0.11}_{-0.03-0.07}$	$3.1^{+1.3+0.6}_{-1.0-0.6}$	3
170	350-500	1000+	9+	3+	$0.81^{+0.56+0.14}_{-0.41-0.14}$	$0.96^{+0.54+0.16}_{-0.27-0.16}$	$0.77^{+0.27+0.53}_{-0.20-0.58}$	$1.3^{+0.2+1.5}_{-0.2-1.1}$	$3.8^{+1.1+1.6}_{-0.7-1.3}$	2
171	500-750	500-1000	9+	3+	$0.00^{+0.43+0.00}_{-0.00-0.00}$	$0.03^{+0.46+0.03}_{-0.02-0.03}$	$0.14^{+0.19+0.11}_{-0.09-0.11}$	$0.01^{+0.02+0.01}_{-0.01-0.00}$	$0.18^{+0.91+0.11}_{-0.09-0.11}$	0
172	500-750	1000+	9+	3+	$0.00^{+0.48+0.00}_{-0.00-0.00}$	$0.53^{+0.56+0.13}_{-0.31-0.13}$	$0.48^{+0.22+0.33}_{-0.16-0.37}$	$0.13^{+0.14+0.15}_{-0.13-0.00}$	$1.1^{+1.1+0.4}_{-0.4-0.4}$	3
173	750+	750-1500	9+	3+	$0.00^{+0.50+0.00}_{-0.00-0.00}$	$0.00^{+0.46+0.00}_{-0.00-0.00}$	$0.00^{+0.09+0.00}_{-0.00-0.00}$	$0.01^{+0.05+0.02}_{-0.01-0.00}$	$0.01^{+0.97+0.02}_{-0.01-0.00}$	0
174	750+	1500+	9+	3+	$0.00^{+0.42+0.00}_{-0.00-0.00}$	$0.00^{+0.46+0.00}_{-0.00-0.00}$	$0.00^{+0.11+0.00}_{-0.00-0.00}$	$0.02^{+0.05+0.02}_{-0.02-0.00}$	$0.02^{+0.89+0.02}_{-0.02-0.00}$	0

Table B.6: Observed number of events and prefit background predictions in the aggregate search regions. The first uncertainty is statistical and second systematic.

Region	$H_{\text{T}}^{\text{miss}}$ [GeV]	H_{T} [GeV]	N_{jet}	$N_{\text{b-jet}}$	Lost-e/μ	$\tau \to$ had	$Z \to \nu\bar{\nu}$	QCD	Total pred.	Obs.
1	>500	>500	$\geq$2	0	842^{+25+48}_{-25-46}	753^{+16+65}_{-16-65}	$5968^{+48+360}_{-47-350}$	$21.4^{+0.6+8.5}_{-0.6-7.1}$	$7584^{+63+370}_{-62-360}$	7838
2	>750	>1500	$\geq$3	0	$4.8^{+2.2+0.6}_{-1.6-0.6}$	$4.2^{+1.3+0.3}_{-0.9-0.3}$	$45.8^{+5.1+5.2}_{-4.3-4.9}$	$0.47^{+0.06+0.18}_{-0.06-0.16}$	$55.2^{+6.2+5.3}_{-5.0-4.9}$	71
3	>500	>500	$\geq$5	0	$111.0^{+6.4+8.3}_{-6.3-7.9}$	$127.6^{+5.9+8.5}_{-5.7-8.6}$	558^{+15+36}_{-14-34}	$9.4^{+0.2+3.5}_{-0.2-3.1}$	806^{+19+38}_{-18-37}	819
4	>750	>1500	$\geq$5	0	$1.82^{+0.82+0.26}_{-0.59-0.21}$	$2.8^{+1.1+0.2}_{-0.7-0.2}$	$18.1^{+3.3+2.7}_{-2.6-2.6}$	$0.37^{+0.06+0.15}_{-0.06-0.13}$	$23.0^{+3.8+2.7}_{-2.9-2.6}$	25
5	>750	>1500	$\geq$9	0	$0.23^{+0.27+0.14}_{-0.17-0.07}$	$0.28^{+0.50+0.08}_{-0.21-0.07}$	$0.00^{+0.82+0.00}_{-0.00-0.00}$	$0.05^{+0.03+0.02}_{-0.03-0.02}$	$0.6^{+1.1+0.2}_{-0.4-0.1}$	1
6	>500	>500	$\geq$2	$\geq$2	$46.9^{+8.9+3.1}_{-5.9-3.0}$	$44.0^{+4.4+3.2}_{-3.4-3.2}$	102^{+2+14}_{-1-14}	$2.5^{+0.3+1.5}_{-0.2-1.3}$	196^{+13+15}_{-9-15}	216
7	>750	>750	$\geq$3	$\geq$1	$11.5^{+4.1+1.0}_{-2.2-0.9}$	$13.7^{+3.0+1.2}_{-2.0-1.2}$	87^{+3+10}_{-3-10}	$0.87^{+0.15+0.34}_{-0.11-0.31}$	113^{+8+10}_{-5-10}	123
8	>500	>500	$\geq$5	$\geq$3	$6.6^{+3.3+0.6}_{-2.3-0.6}$	$5.3^{+1.9+0.9}_{-1.1-0.9}$	$6.8^{+0.5+2.8}_{-0.3-2.8}$	$0.87^{+0.20+0.96}_{-0.17-0.70}$	$19.5^{+5.2+3.2}_{-3.4-3.1}$	17
9	>750	>1500	$\geq$5	$\geq$2	$1.3^{+1.4+0.2}_{-0.6-0.2}$	$1.8^{+1.3+0.4}_{-0.7-0.4}$	$1.20^{+0.41+0.33}_{-0.19-0.33}$	$0.13^{+0.07+0.06}_{-0.04-0.05}$	$4.4^{+2.8+0.6}_{-1.3-0.6}$	6
10	>750	>750	$\geq$9	$\geq$3	$0.00^{+0.66+0.00}_{-0.00-0.00}$	$0.00^{+0.65+0.00}_{-0.00-0.00}$	$0.00^{+0.15+0.00}_{-0.00-0.00}$	$0.03^{+0.07+0.04}_{-0.02-0.01}$	$0.0^{+1.3+0.0}_{-0.0-0.0}$	0
11	>300	>300	$\geq$7	$\geq$1	328^{+12+21}_{-12-20}	380^{+10+22}_{-9-22}	193^{+8+38}_{-6-38}	69^{+1+29}_{-1-26}	969^{+23+57}_{-22-55}	890
12	>750	>750	$\geq$5	$\geq$1	$7.2^{+2.8+0.8}_{-1.6-0.7}$	$7.7^{+2.4+0.8}_{-1.4-0.8}$	$26.6^{+2.4+3.9}_{-1.8-3.7}$	$0.65^{+0.14+0.26}_{-0.11-0.23}$	$42.2^{+5.7+4.0}_{-3.5-3.9}$	48